

Review

# Circumstellar and circumbinary discs in multiple stellar systems

Nicolás Cuello <sup>1,†</sup>, Antoine Alaguero <sup>1,†</sup> and Pedro P. Poblete <sup>1</sup><sup>1</sup> Univ. Grenoble Alpes, CNRS, IPAG, 38000 Grenoble, France\* Correspondence: [nicolas.cuello@univ-grenoble-alpes.fr](mailto:nicolas.cuello@univ-grenoble-alpes.fr), [antoine.alaguero@univ-grenoble-alpes.fr](mailto:antoine.alaguero@univ-grenoble-alpes.fr).

† These authors contributed equally to this work.

**Abstract:** The interplay between stellar multiplicity and protoplanetary discs represents a cornerstone of modern astrophysics, offering key insights into the processes of planet formation. Protoplanetary discs act as cradles for planetary systems, yet their evolution and capacity to form planets are profoundly affected by gravitational forces within multiple stellar systems. This review synthesises recent advancements in observational and theoretical studies to explore the rich diversity of circumstellar and circumbinary discs within multiple stellar systems. We examine how stellar companions shape disc morphology through truncation, spirals, and misalignment. We also outline how dust dynamics and planetesimal formation are impacted by stellar multiplicity. On top of this, observations at high angular resolution reveal detailed disc structures, while simulations offer key insights into their evolution. Last, we consider the implications of stellar multiplicity for planetary system architectures, emphasising the diversity of planetary outcomes in such environments. Looking ahead, coordinated efforts combining high-resolution observations with advanced numerical models will be critical for unravelling the role of multiple stellar systems in shaping planetary formation and evolution.

**Keywords:** Protoplanetary Discs; Stellar Multiplicity; Planet Formation; Binary Stars; Astronomical Observations; Hydrodynamical Simulations; Exoplanets

## 1. Introduction

The formation of stars and planets is intimately linked through the physical processes that unfold within protoplanetary discs, which are rotating structures of gas and dust that surround young stellar objects [1]. These discs are the cradles of planetary systems where microscopic dust grains are transformed into planetesimals, which eventually evolve into rocky or gaseous planets — depending on their surrounding conditions and migration [2]. The dynamics, structure, and lifetime of these discs are key in determining the diversity of planetary architectures observed in the galaxy. However, a definitive link between protoplanetary discs and the resulting exoplanets has yet to be firmly demonstrated [3]. This topic constitutes an active topic of research in modern-day astrophysics.

In addition, it is now well established that multiple stellar systems are ubiquitous, particularly among young stars [4]. Observational surveys reveal that around 65% of stars are born not in isolation but as members of binary or higher-order multiple systems [5,6]. In fact, the prevalence of stellar multiplicity raises fundamental questions about its influence on protoplanetary discs. How do interactions between stellar companions shape the distribution and evolution of gas and dust? To what extent do these interactions enhance or hinder planet formation? Are planetary systems in multiples different from the ones around single stars? All in all, multiple stellar systems represent astrophysical laboratories of great scientific value if one wishes to decipher the process of planet formation.

When considering discs in multiple stellar systems, it is essential to distinguish between circumstellar discs (surrounding individual stars in a system) and circum-multiple discs (encircling two or more stars at the centre). For instance, Figure 1 shows the maximum



**Citation:** Cuello, N.; Alaguero, A.; Poblete, P.P. Discs in multiple stellar systems. *Symmetry* **2024**, *1*, 0. <https://doi.org/>

Received: 25 Nov 2024

Revised: 21 Dec 2024

Accepted: 25 Dec 2024

Published:



**Copyright:** © 2024 by the authors. Licensee MDPI, Basel, Switzerland. This article is an open access article distributed under the terms and conditions of the Creative Commons Attribution (CC BY) license (<https://creativecommons.org/licenses/by/4.0/>).

number of discs within hierarchical multiple systems<sup>1</sup>: 1 for singles, 3 for binaries, and up to 5 for triples. These configurations differ not only in their geometrical setup but also in their formation histories, dynamical behaviour, and long-term evolution [4,7,8]. Circumstellar discs may experience truncation and gravitational perturbations due to the presence of an external stellar companion [9,10], while circumbinary and circumtriple discs are shaped by the motion of the stars within their inner cavity [11,12]. If we consider multiple stellar systems in hierarchical arrangements, to first order, triple and quadruple systems can often be approximated as binary systems. Based on this observation, here, we will primarily address circumstellar and circumbinary discs — mentioning when relevant the detailed orbital arrangement of a given system.

This review aims to explore the rich diversity of protoplanetary discs in multiple stellar systems, focusing on their distinct formation pathways, dynamical interactions, and implications for planet formation. By synthesising recent observations and theoretical advances, we seek to highlight the critical role that stellar multiplicity plays in shaping the architecture of planetary systems. In Section 2 we present the orbital elements and typical parameters used to describe and model stars and discs in multiples. Then, in Sections 3 and 4, we give an overview of the processes governing the dynamics in discs of multiple stellar systems and summarise recent observations of circumstellar and circumbinary discs in multiples (respectively). Finally, in Section 5, we discuss these observations in the context of planet formation theories, and we list our conclusions in Section 6.



**Figure 1.** Possible types of protoplanetary discs in systems with one star (left), two stars (centre), and three stars (right): circumstellar, circumbinary, or circumtriple. For simplicity, we show hierarchical stellar configurations only. For clarity, the circumstellar discs are shown in edge-on configurations.

## 2. Orbital parameters and typical disc parameters

To describe stellar orbits alongside the dynamics and structure of discs in multiple stellar systems, we first introduce key concepts in celestial mechanics (Sect. 2.1) and protoplanetary disc models (Sect. 2.2). This will provide a useful framework for analysing individual disc observations and understanding the underlying physical mechanisms.

### 2.1. Orbital characterisation

Traditionally, the orbital parameters used to describe the motion of a two-body system bound by gravity are defined relative to the centre of mass. These parameters are the semi-major axis ( $a$ ), the eccentricity ( $e$ ), the inclination ( $i$ ), the longitude of the ascending node ( $\Omega$ ), the argument of periaxis ( $\omega$ ), and the true anomaly ( $v$ ). All these parameters are shown in Fig. 2 and we provide a detailed explanation in Appendix A. For a specific

<sup>1</sup> A hierarchical multiple system refers to a stellar configuration in which the system can be divided into nested subsystems, each gravitationally bound and dynamically stable over long timescales. For instance, a triple system can consist of a close binary orbited by a third star at a much larger distance. The stability of such systems arises because the gravitational interactions between stars within each subsystem dominate over interactions between different subsystems.

system, the values of these parameters determine the discs' sizes and the type of alignment or oscillations that circumstellar and circumbinary discs can undergo. For instance, the value of the binary semi-major axis  $a$  puts strong constraints on circumstellar disc sizes and on circumbinary disc inner cavities. The process of polar alignment of a circumbinary can only occur if the inner binary orbital eccentricity verifies  $e > 0$  [13–15]. Also, the closer  $\Omega$  gets to  $90^\circ$ , the more likely the process of polar alignment becomes [13,16]. Last, the binary inclination  $i$  critically determines the precession rate and oscillation evolution of misaligned discs [17].

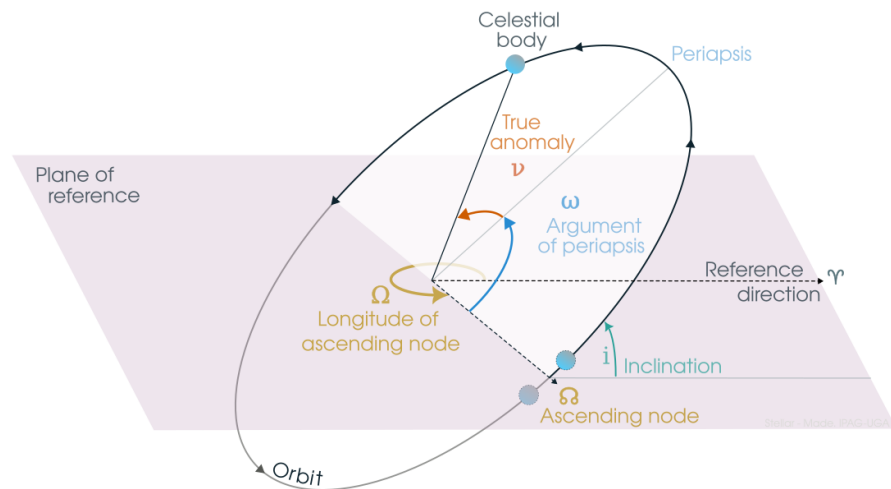


**Figure 2.** Schematic illustration of the orbital parameters for an elliptical orbit: the inclination  $i$ , the argument of periaxis  $\omega$ , the longitude of the ascending node  $\Omega$ , and the true anomaly  $v$ . Provided through the courtesy of Mario Sucerquia.

The orbital parameters of multiple stellar systems can be precisely constrained through high-precision astrometric observations conducted over extended periods with instruments such as VLT/GRAVITY [18], VLT/SPHERE [19] and Karl G. Jansky Very Large Array (VLA). This detailed characterisation is critical for linking stellar motions to the structures observed in protoplanetary discs. This integrated approach not only bridges observational data with theoretical models but also enhances our understanding of how stellar orbits influence disc behaviour and, ultimately, planet formation. For instance, the values of the binary mass ratio  $q$  and  $(a, e, i)$  strongly impact the morphology and evolution of the inner cavity of circumbinary discs [20–24]. Relative misalignments between stellar and disc orbital planes can also indicate the oscillation regime of a given disc in a multiple stellar systems [15,25–27]. Last, disc substructure in the form of spirals and over-densities can be directly related to different sets of binary orbital parameters. This last connection is better established through detailed hydrodynamical simulations for several hundreds or thousands binary orbital periods [21,28–33]. For instance, recent works on the multiple stellar system GG Tau [27,34] present disc dynamics simulations done with great accuracy using updated astronomical constraints — shedding light on the complex ongoing interactions. In the following section, we outline the fundamental equations governing the evolution of protoplanetary discs.

## 2.2. Protoplanetary discs characterisation

Protoplanetary discs are rotating structures made of gas and solid material that surround young stars, with gas being the dominant component (exceeding the solid material by at least an order of magnitude, [35]). This gas-dominated nature allows protoplanetary discs to be treated as fluids, requiring the use of hydrodynamical equations for accurate modelling. In this context, the Navier-Stokes equations are fundamental to describe the

fluid motion around young stars — though they remain unsolved in their general form. Therefore, we must rely on simplifying assumptions and approximations to write the governing equations of protoplanetary discs. Assuming that the fluid is incompressible and follows an adiabatic equation of state, these equations can be written as follows:

$$\text{Mass conservation: } \frac{\partial \rho}{\partial t} + \rho(\nabla \cdot \mathbf{v}) = 0, \quad (1)$$

$$\text{Momentum conservation: } \frac{d\mathbf{v}}{dt} = -\frac{\nabla P}{\rho} + \Pi_{\text{shock}} + \mathbf{a}_{\text{grav}}, \quad (2)$$

$$\text{Energy conservation: } \frac{du}{dt} = \frac{P}{\rho^2} \frac{d\rho}{dt} + \Lambda_{\text{shock}} - \frac{\Lambda_{\text{cool}}}{\rho}, \quad (3)$$

$$\text{Equation of state: } P = (\gamma - 1)\rho u. \quad (4)$$

Here,  $\rho$  denotes the gas density,  $\mathbf{v}$  is the local fluid velocity vector,  $P$  represents the gas pressure,  $u$  is the gas internal energy, and  $\gamma$  is the adiabatic index. The term  $\mathbf{a}_{\text{grav}}$  accounts for external gravitational acceleration due to stars, planets, or the disc's self-gravity. Additionally,  $\Pi_{\text{shock}}$  includes an effective shock-viscous contribution designed to capture discontinuities at shocks [2,36]. More precisely, it is a vector arising from the divergence of a shock-viscous stress tensor, added in many numerical methods to suppress unphysical oscillations near steep gradients [36,37]. Its dissipative counterpart in the energy equation is  $\Lambda_{\text{shock}}$ , which represents the conversion of kinetic energy into heat wherever shocks are present. Formally,  $\Lambda_{\text{shock}}$  is derived from the same artificial-viscosity or effective-viscosity approach used to construct  $\Pi_{\text{shock}}$ , ensuring that momentum and energy are treated self-consistently in shock regions. Meanwhile,  $\Lambda_{\text{cool}}$  encompasses radiative and other cooling processes. Together, these parameters encapsulate the fundamental physical processes governing protoplanetary discs. This framework can be easily expanded to include additional terms when other physical processes are relevant (e.g., ionisation from the interstellar medium, electromagnetic effects, gas chemistry; [38]).

With these four fundamental equations in mind, power-laws are often used to model the radial surface density and temperature profiles:  $\Sigma(r) = \Sigma_0(r/r_0)^{-p}$  and  $T(r) = T_0(r/r_0)^{-q}$ , where  $r_0$  is a reference radius, and  $\Sigma_0$  and  $T_0$  are constants. In addition, the gas vertical density structure typically follows:  $\rho(z) = \rho_0 \exp(-z^2/(2h^2))$ , where  $z$  is the vertical cylindrical coordinate,  $h$  is the scale height,  $q$  is the power-law index, and  $\rho_0$  is a constant. This Gaussian profile arises from the assumption of hydrostatic equilibrium in the vertical direction, where the vertical pressure gradient is balanced by the gravitational force. Mathematically, this balance leads to an exponential decline of the density with height, with  $h$  determined by the thermal properties of the gas and the mass of the central star [2]. Under such assumptions, all these parameters are linked to the total mass of the disc, which is challenging to estimate observationally. The typical disc-to-star mass ratios range from 1% to 20% [1,39], though these values may vary for discs in multiple stellar systems. A caveat of the vertical isothermal assumption is that it inherently neglects the vertical thermal stratification expected in discs, which plays a crucial role in shaping their dynamical, dust, and chemical processes [e.g. 40–42].

Gas is the most abundant component of the disc, but dust (though less prevalent) plays a pivotal role in regulating opacity, forming solid cores, and influencing chemical abundances. The exact gas-to-dust ratio in a protoplanetary disc is not precisely known but is often assumed to resemble that of the interstellar medium, with a typical dust-to-gas ratio of 0.01 [43]. The solid material mainly consists of silicate dust grains, which vary widely in size and shape [e.g. 44]. Size is particularly significant when modelling gas-dust interactions, as the grain size distribution is assumed to follow a power law with an index  $m$  defined by equation 5 below:

$$\frac{dn}{ds} = s_0 s^{-m}, \quad (5)$$

where  $n$  is the number of particles with radius  $s$ , and  $s_0$  is a normalisation constant. The standard value for  $m$  measured in the interstellar medium is 3.5, indicating that smaller particles are more abundant than larger ones [45]. Grain sizes range from 0.01  $\mu\text{m}$  to centimetre scales, while particles exceeding metre sizes are often categorised as solid cores or embryos. The disc's optical properties are dominated by small grains, whereas the majority of the mass resides in larger grains [39].

In protoplanetary discs, dust particles interact with the surrounding gas exchanging angular momentum and typically evolving under the Epstein regime, in which the mean free path of gas molecules exceeds the particle size [46]. From the physical point of view, a dust grain in motion within the disc experiences an aerodynamic drag force proportional to the velocity difference between the grain and the gas. With the gas orbiting at a sub-Keplerian frequency due to pressure forces, the dust grains orbiting at a Keplerian frequency start to drift toward the star and to settle in the mid-plane of the disc [47,48]. The degree of coupling between dust and gas, characterized by the Stokes number  $\text{St}$ , governs dust evolution and distribution within the disc. Particles strongly coupled to the gas ( $\text{St} \ll 1$ ) follow the gas flow, while decoupled particles ( $\text{St} \gg 1$ ) move independently in Keplerian orbits. Marginally coupled particles ( $\text{St} \sim 1$ ) experience the maximum radial drift, a key factor in determining dust concentration and growth. Instruments like SPHERE<sup>2</sup> can trace the stellar light scattered by small grains tightly coupled to the gas [49], while instrument like ALMA<sup>3</sup> probe the thermal emission of grains with sizes close to the millimetre [50].

### 3. Circumstellar discs (CSDs) in multiple stellar systems

Circumstellar discs in multiple stellar systems are heavily influenced by gravitational perturbations from nearby stellar companions, which profoundly impact their structure, dynamics, and evolution. In the following, we briefly outline the key mechanisms at play and present a limited but representative selection of circumstellar discs in such systems.

#### 3.1. Tidal truncation of CSDs

In binary and multiple stellar systems, circumstellar discs experience tidal truncation due to the gravitational influence of nearby stellar companions. This process occurs as the torque exerted by the outer companion limits the radial extent of the disc, effectively *truncating* its size [9,10]. The truncation radius depends on the mass ratio and separation of the stars, as well as the orbital configuration of the system. As a result, circumstellar discs in these systems are typically smaller than those around isolated stars [e.g. 51–54]. Beyond reducing the size of the disc, tidal truncation also steepens the radial surface density profile of the gas [55–57]. This change in density has significant implications for the evolution of solids within the disc. A steeper surface density profile increases the pressure gradient, which in turn accelerates the radial drift of dust and larger particles toward the central star [55,58,59]. This enhanced drift can deplete the disc of solids more quickly, potentially stifling planet formation processes.

As a consequence, circumstellar discs in multiple stellar systems are thought to have shorter lifespans compared to their counterparts around single stars [60–62]. However, this limitation may be mitigated if the discs are resupplied with material from external reservoirs. Such reservoirs could include circumbinary discs, infalling envelopes, or streamers that channel material inward. These mechanisms may play a crucial role in sustaining circumstellar discs in the presence of tidal truncation, thereby extending their lifetimes and maintaining conditions suitable for planet formation (see Sects. 4 and 5).

<sup>2</sup> The Spectro-Polarimetric High-Contrast Exoplanet Research (SPHERE) instrument, mounted on the Very Large Telescope (VLT) in Chile, is optimized for high-resolution imaging and polarimetric observations, particularly in scattered light, to study circumstellar environments and exoplanets.

<sup>3</sup> The Atacama Large Millimeter/submillimeter Array (ALMA) is an interferometric radio telescope located in Chile, designed for high-resolution observations of dust, gas, and other structures in protoplanetary discs and the interstellar medium.

### 3.2. Structure formation in CSDs

Gravitational interactions between a disc and a nearby stellar companion can lead to the emergence of striking structures within the disc, with spiral density waves being one of the most prominent examples [4,63]. These waves are launched at Lindblad resonances [64], where the companion's gravitational influence perturbs the disc material, generating density waves that propagate through the gas and dust [65]. The morphology of the spirals depends on a combination of parameters, including the companion's mass and orbital separation, as well as the disc's properties, such as viscosity, cooling efficiency, and thickness [66,67]. High-mass companions or close-in perturbers tend to produce more prominent and tightly wound spirals, while discs with higher cooling efficiency exhibit sharper and more defined features. These spirals are observable across different tracers, with scattered light revealing the fine structures in the disc's upper layers [49], molecular line emission tracing gas kinematics [68], and dust thermal emission highlighting the denser mid-plane regions (e.g., HD 100453, [29]; AS 205, [69]; [50]).

The interaction between a companion and a disc not only generates spirals but can also drive material outward, where it may circularise and form transient circumstellar discs (CSDs) around the companion. This process is more likely to occur in unbound encounters, also known as flybys, where the perturber does not remain gravitationally bound to the system [70,71]. In such cases, the companion's interaction can eject substantial material from the disc, some of which may accumulate around the perturber. In contrast, for bound companions, the spirals are periodically excited with each orbit, although their amplitude diminishes over time as the disc is truncated and its mass redistributed [e.g., 72]. Consequently, the formation of second-generation circumstellar discs around the perturber is unlikely in bound systems.

### 3.3. CSD alignment

The alignment of circumstellar discs (CSDs) in binary and multiple stellar systems is influenced by the gravitational interactions between the stars and the disc. When the orbital plane of the companion star is inclined relative to the plane of the disc, the disc experiences torques that can induce oscillations in its inclination. These oscillations occur around an equilibrium plane determined by the total angular momentum of the system, which combines the angular momenta of the stars and the disc(s). The amplitude and frequency of these oscillations strongly depend on the system's orbital parameters: the companion's mass, separation, inclination, and orbital eccentricity; as well as the disc mass, radial extent, viscosity, and thickness [73,74].

In many configurations, the disc may begin to precess around the angular momentum vector of the entire stellar system. This precession can occur either differentially, where individual disc annuli precess at different rates, or as a solid body, where the entire disc precesses uniformly. The mode of precession depends on the balance between wave-like communication (dominated by sound speed and pressure forces) and viscous timescales within the disc [75]. For thin, inviscid discs, differential precession is common, with the precession rate varying as  $a^{3/2}$ , where  $a$  is the radial distance from the central star. In contrast, thick or highly viscous discs are more likely to exhibit solid-body precession.

In systems with strongly inclined or eccentric orbits, the interaction can drive more complex dynamics. For instance, the disc may undergo Kozai-Lidov-like oscillations, where the disc inclination and eccentricity oscillate periodically due to the influence of the companion's gravitational potential [76]. These oscillations can lead to significant warping or disc breaking if the companion's torque overcomes the internal forces maintaining the disc's structure [77]. Over time, the dissipation of energy through viscosity may lead to alignment or misalignment between the disc and the orbital plane of the companion star, depending on the system's initial configuration [74]. Viscous forces within the disc act to damp oscillations, promoting alignment with the total angular momentum vector of the system. However, in some cases, the initial conditions and ongoing perturbations can result in persistent misalignment, which is observed in several multiple stellar systems [7,78,79].

### 3.4. CSDs of interest

In the following, we describe ALMA and SPHERE observations of multiple stellar systems harbouring circumstellar discs in an attempt to illustrate the interactions between a disc and an external companion. We list these systems in Table 1 and show a gallery of recent observations in Figure 3. The SPHERE polarimetric data were downloaded from the ESO archive<sup>4</sup> and then processed using the IRDAP open-access pipeline<sup>5</sup>. The images shown are in polarized intensity with the contribution of the central star removed<sup>6</sup>. The ALMA images displayed in the galleries below are "quality assurance" products that were downloaded from the ALMA archive<sup>7</sup> and used as they are.

**Table 1.** Multiple stellar systems of interest with protoplanetary discs.

Name	RA (hh:mm:ss)	Dec (dd:mm:ss)	Number of stars	Type of disc(s) <sup>1</sup>	References
HT Lup	15:45:12.868	-34:17:30.64	3	CSD	[81,82]
S CrA	19:01:08.597	-36:57:19.90	2	CSD	[83,84]
UY Aur	04:51:47.389	+30:47:13.55	2	CSD	[85,86]
T Tau	04:21:59.432	+19:32:06.43	3	CSD,CBD	[87]
HD 100453	11:33:05.577	-54:19:28.55	2	CSD	[88,89]
UZ Tau	04:32:43.022	+25:52:30.90	4	CSD,CBD	[87,90]
GG Tau	04:32:30.351	+17:31:40.49	5	CSD,CTD	[91–97]
GW Ori	05:29:08.393	+11:52:12.67	3	CBD,CTD	[98–101]
HD 142527	15:56:41.888	-42:19:23.25	2	CSD,CBD	[102–105]
HD 98800	11:22:05.290	-24:46:39.76	4	CBD	[106,107]

Table B1 in Appendix B presents a more complete sample of multiple stellar systems with discs.

<sup>1</sup> CSD : CircumStellar Disc, CBD : CircumBinary Disc, CTD : CircumTriple Disc

**HT Lup.** Located at a distance of  $154 \pm 2$  pc [108], the HT Lup system comprises three stars, all detected in millimetre wavelengths through both continuum and CO emission. HT Lup AB forms a close binary with a separation of  $\sim 0.1''$ , while HT Lup C is positioned  $\sim 3''$  to the west, making the system a hierarchical triple. The individual discs around HT Lup A and HT Lup B were first resolved by the DSHARP survey [69,82]. The primary disc is relatively compact ( $r \sim 30$  au), while the secondary disc is only marginally resolved, suggesting truncation of both discs due to gravitational interactions. Interestingly, if the projected separation of HT Lup AB is assumed to represent the semi-major axis of a coplanar binary with an eccentricity of 0.2, the expected truncation radius of the primary disc would be just 16 au [10]. This discrepancy, along with the absence of material connecting the two discs, implies that the true separation of HT Lup A and HT Lup B is likely larger along the line of sight [69]. Despite this, distinct spiral features in the continuum emission of HT Lup A suggest recent tidal interactions. Furthermore, CO intensity maps reveal that the primary and secondary discs are counter-rotating [69], suggesting the possibility of a retrograde orbit for HT Lup AB.

**S CrA.** S CrA is a binary system with component masses of  $0.70 M_{\odot}$  and  $0.45 M_{\odot}$  [109], separated by  $\sim 1''$ . The individual circumstellar discs have been imaged in the near-infrared (NIR) [110], in continuum emission [84], and in CO lines [111]. In the continuum, the discs appear compact, while NIR observations reveal material connecting the two discs and extending into their surrounding environment. Recent analysis of NIR observations

<sup>4</sup> [http://archive.eso.org/eso/eso\\_archive\\_main.html](http://archive.eso.org/eso/eso_archive_main.html)

<sup>5</sup> <https://irdap.readthedocs.io/>

<sup>6</sup> Polarimetric observations of discs in multiple stellar systems are challenging due to the contamination of the signal by nearby stars, see [80] for more details.

<sup>7</sup> <https://almascience.eso.org/aq/>

by [110] identified spiral features in the primary disc, along with a tentative ring structure. Using astrometric measurements, the authors suggested an orbital inclination of  $i = 25 \pm 12^\circ$ , which aligns with the plane of the inner disc but not with the inclination of  $\sim 57^\circ$  determined for the outer disc [18]. While the observed spiral arms may result from tidal interactions with the secondary companion, alternative explanations include interactions with surrounding or infalling gas. These processes could also account for the diffuse emission observed in the environment of the binary system [111,112].

**UY Aur.** Located in the Taurus–Aurigae star-forming region, UY Aur consists of at least two stars of mass  $0.6 M_\odot$  and  $0.34 M_\odot$  separated by  $0.88''$  [113]. A potential close companion to UY Aur B has been proposed to explain its photometric variability [86]. Early scattered-light and gas emission images of the system reveal extended circumbinary material, while millimetre emission clearly traces the individual discs associated with each star [86,114]. However, the rotation pattern observed in the circumbinary gas emission deviates from Keplerian motion, complicating the identification of a rotationally supported circumbinary disc [57]. The dust discs in UY Aur are among the most compact in the Taurus region, likely due to significant tidal truncation [51,115]. Scattered-light and gas emission in the surrounding environment show numerous arc-like structures, which may result from interactions between the stars, the discs, and the out-flowing material [116,117]. Further constraints on the orbit of UY Aur AB are necessary to robustly link these observed structures to the binary's dynamics and better understand the system's evolution.

**T Tau.** T Tau is one of the brightest optical objects in the Taurus cloud and is a triple stellar system. It consists of a  $2.2 M_\odot$  star (T Tau N) orbiting a close binary (T Tau S) with component masses of  $2.1 M_\odot$  and  $0.4 M_\odot$  [118,119]. High-resolution continuum imaging detected emission associated with each of the three stars [120]. T Tau N harbours a disc of  $\sim 22$  au, which features an apparent gap, while T Tau Sa and T Tau Sb host very compact discs. The orbit of the T Tau S binary has been well characterized, and its orbital period correlates strongly with arc-like structures observed to the south of the system [119,121]. However, the kinematics of the T Tau system are complex, likely reflecting interactions between the stars and surrounding infalling and out-flowing material [121,122]. Based on modelling of 1.3 mm continuum images, the presence of a circumbinary disc (CBD) around T Tau S was proposed [121]. Notably, neither the individual discs nor the potential CBD associated with T Tau S appear to be aligned with the binary's orbital plane [119–121].

**HD 100453.** Located in the Lower Centaurus Association [123], HD 100453 is a Herbig star with a mass of  $1.7 M_\odot$  and a nearby  $0.2 M_\odot$  companion situated  $\sim 1''$  to the south-east [88]. The disc has been observed in near-infrared (NIR), millimetre continuum emission, and gas tracers [124–126]. These observations reveal a large cavity in the dust emission and an azimuthal asymmetry in the north-east, interpreted as the dust counterpart of extended spiral arms seen in the NIR and CO emission. HD 100453 has been extensively modelled to explain the origin of its spiral structures [29,124–129]. The favoured interpretation attributes the spirals to tidal interactions with the companion, HD 100453 B. Both astrometric fitting and forward modelling of the disc structures suggest a misaligned orbit between the binary and the disc, which likely causes the disc to precess [29]. Additionally, shadows observed in the NIR may indicate the presence of a misaligned inner disc. This scenario suggests that an undetected inner companion could have carved the cavity, dynamically decoupling the inner and outer discs [130].

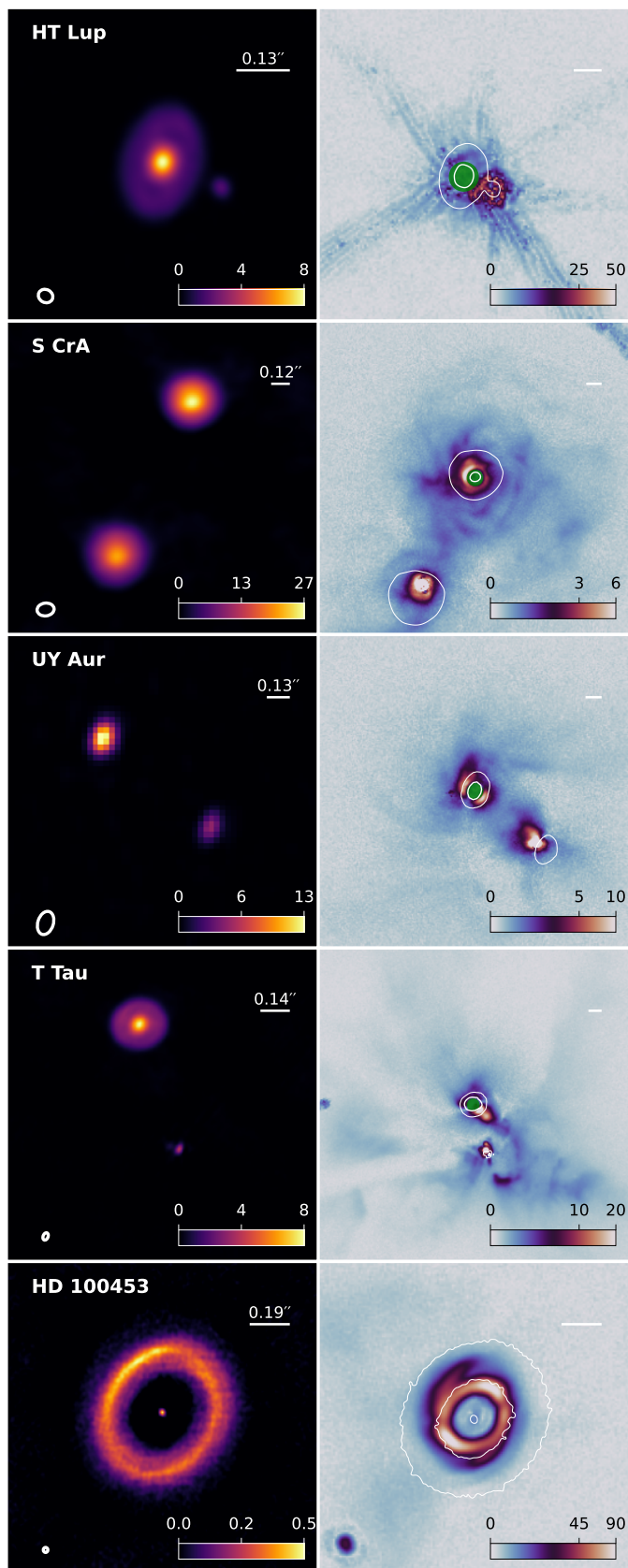


**Figure 3.** Gallery of observed circumstellar discs (CSDs) with external companions. Left column: ALMA 1.3 mm intensity maps (mJy/beam) with the synthesized beam and a 20 au scale bar (angular size noted). Right column: SPHERE polarized intensity data (% of peak value) processed with IRDAP, showing a 20 au scale bar and a green circle for the coronagraph position, if used. SPHERE data are at 1.65  $\mu$ m, except 2.15  $\mu$ m for HD 100453. White contours show ALMA 1.3 mm emission at  $[5, 50]\sigma$ , centred on the coronagraph or primary star.

#### 4. Circumbinary discs (CBDs) in multiple stellar systems

Circumbinary discs (CBDs) in binary and multiple stellar systems represent complex and dynamic environments where interactions between the central binary and the disc strongly influence its structure and evolution. Unlike CSDs, which are directly associated with individual stars, CBDs encircle the entire binary system, and their morphology is shaped by the combined gravitational potential of the central stars. These discs are critical for understanding angular momentum transfer, accretion processes, and the formation of planets in binary systems.

##### 4.1. Size and shape of the inner CBD cavity

One of the most distinctive features of a CBD is its large inner cavity, which forms due to tidal torques exerted by the binary. These torques prevent material from accreting directly onto the central stars, resulting in a cleared region whose size depends on the binary's orbital separation, mass ratio, and eccentricity. For circular binaries, the cavity radius is typically 2 – 3 times the binary separation, while eccentric binaries carve larger cavities, with sizes scaling approximately with  $(1 + e)$  [11].

The cavity shape in circumbinary discs is determined by the binary's orbital parameters. For instance, CBDs with inner binaries with mass ratios high enough ( $q = M_2/M_1$  above 0.05) develop eccentric disc cavities — both for circular and eccentric binaries [12,21,23,32]. This mechanism eventually leads to the formation of lopsided (horseshoe-shaped) structures. These azimuthal asymmetries can translate into density enhancements, which are observable in gas tracers and dust continuum emission [e.g., 24,31,131]. The dynamics within the cavity itself are complex, with material often flowing toward the stars via streamers that bridge the cavity [132–134]. These accretion flows are essential for sustaining circumstellar material in binary systems, influencing accretion rates onto the stars and modulating binary evolution.

##### 4.2. Structure formation in CBDs

Gravitational torques exerted by the binary also drive the formation of structures such as spiral density waves and large-scale azimuthal asymmetries in CBDs. Unlike spirals in circumstellar discs, which are driven by external companions, spirals in CBDs are launched by the central binary itself. These features are most prominent in gas tracers, where density waves propagate outward from Lindblad resonances within the disc. The morphology of these spirals is influenced by the binary's orbital parameters, including mass ratio and eccentricity, as well as the disc's thermodynamic properties like viscosity and cooling efficiency [21,28,32].

Azimuthal asymmetries in the disc, such as horseshoe-shaped dust accumulations or lopsided gas structures, may arise from gravitational resonances or pressure traps at the inner cavity edge [20,22]. These features are observable in dust thermal emission and scattered light and may serve as sites for planetesimal growth. Additionally, simulations suggest that these structures may be transient or long-lived, depending on the binary's stability and the disc's physical properties [12].

##### 4.3. CBD alignment

The alignment of a CBD with the orbital plane of the binary depends on the binary's inclination, mass ratio, and eccentricity, as well as the disc's viscosity and angular momentum. Misaligned CBDs are often observed, particularly in systems where the binary orbits are themselves inclined relative to the total angular momentum vector of the system (see examples in Sect. 4.4). This misalignment can induce warps or twists in the disc, with different regions of the disc precessing at different rates due to differential torques [17].

For small misalignments, circumbinary discs (CBDs) can align with the binary's orbital plane over time through viscous dissipation [77]. However, if the initial inclination exceeds a critical angle, the disc may enter more complex dynamical regimes. In such cases, the disc can break into multiple misaligned rings or undergo Kozai-Lidov oscillations, where the

disc's inclination and eccentricity oscillate periodically due to the gravitational influence of the binary [14,77,135]. These effects are especially pronounced in systems with high binary eccentricities or weakly viscous discs.

For larger initial misalignments around eccentric binaries, CBDs may also achieve a state of polar alignment, where the disc becomes orthogonal to the binary's orbital plane [13]. This occurs when the binary's eccentricity-driven torques dominate over the viscous forces acting to align the disc with the orbital plane. In this regime, the CBD precesses stably around the binary's eccentricity vector, while being almost in an orthogonal orientation with respect to the binary orbital plane [14–16]. It is worth noting that several CBDs are observed having in an intermediate configuration, neither coplanar nor polar, and that these discs are found most of the time in high-order multiple systems, suggesting additional physics [26,78,136].

CBD misalignment also has significant implications for accretion. In misaligned systems, accretion streams may deliver material to circumstellar discs or directly onto the stars in a non-axisymmetric manner, potentially modulating accretion rates and driving variability in observed emission [133,134,137]. The resulting luminosity variability underscores the role of CBDs in shaping both stellar evolution and the potential for planet formation in these complex environments.

#### 4.4. CBDs of interest

In the following, we describe ALMA and SPHERE observations of multiple stellar systems hosting circumbinary discs. We discuss the observational features of these systems and their interpretation in light of modelling efforts carried out by the community. These systems are listed in Table 1 and we show a gallery of recent observations in Figure 4.

**UZ Tau.** The young stellar system UZ Tau comprises four stars. UZ Tau E is a spectroscopic binary with a total mass of  $1.3 M_{\odot}$ , located  $3.54''$  away from UZ Tau W. The latter consists of two stars separated by  $0.37''$ , with poorly constrained properties [87,138]. ALMA observations reveal a plain circumbinary disc (CBD) around UZ Tau E and two marginally resolved circumstellar discs (CSDs) associated with the stars in UZ Tau W. The sizes of the individual discs in UZ Tau W are consistent with tidal truncation. Moreover, their alignment with each other and the CBD suggests orbital coplanarity [117]. Given the large observed separation between UZ Tau E and W, recent interactions between these components are unlikely. The CBD of UZ Tau E appears coplanar with its inner binary, which is consistent with the binary's moderate eccentricity of  $e = 0.3$  [138,139]. However, contrary to theoretical predictions of a visible cavity of  $\sim 0.3''$  [11], the CBD shows only shows a small inner cavity of  $\lesssim 0.08''$  [140], raising questions about its formation.

**GG Tau.** GG Tau is a hierarchical quintuple stellar system, consisting of GG Tau A (three stars) and GG Tau B (two stars) separated by  $\sim 10''$  [91]. GG Tau A, the more massive subsystem, includes GG Tau Aa and GG Tau Ab with estimated masses of  $0.59 M_{\odot}$  and  $\sim 0.6 + 0.2 M_{\odot}$ , respectively, and well-characterized internal orbits [34,141]. This subsystem hosts a bright and long-studied circumtriple disc (CTD) which surrounds GG Tau A, featuring a prominent central cavity carved by the three stars (often considered as a binary) [e.g., 92,95,142,143]. High-resolution observations reveal asymmetries in the disc, including shadows along the RA axis and material within the cavity, possibly infalling toward the stars [97]. Millimetre-wavelength observations also trace the circumstellar disc of GG Tau Aa [141]. CO emission maps display prominent spiral arms extending into the cavity, which may result from gravitational interactions with GG Tau B or the inner stars of GG Tau A [68,141]. The discs associated with GG Tau Ab and a potential CBD remain undetected, likely due to tidal truncation reducing their sizes. Modelling efforts suggest a misaligned configuration between the CBD and GG Tau A, which could explain some of the observed features [27].

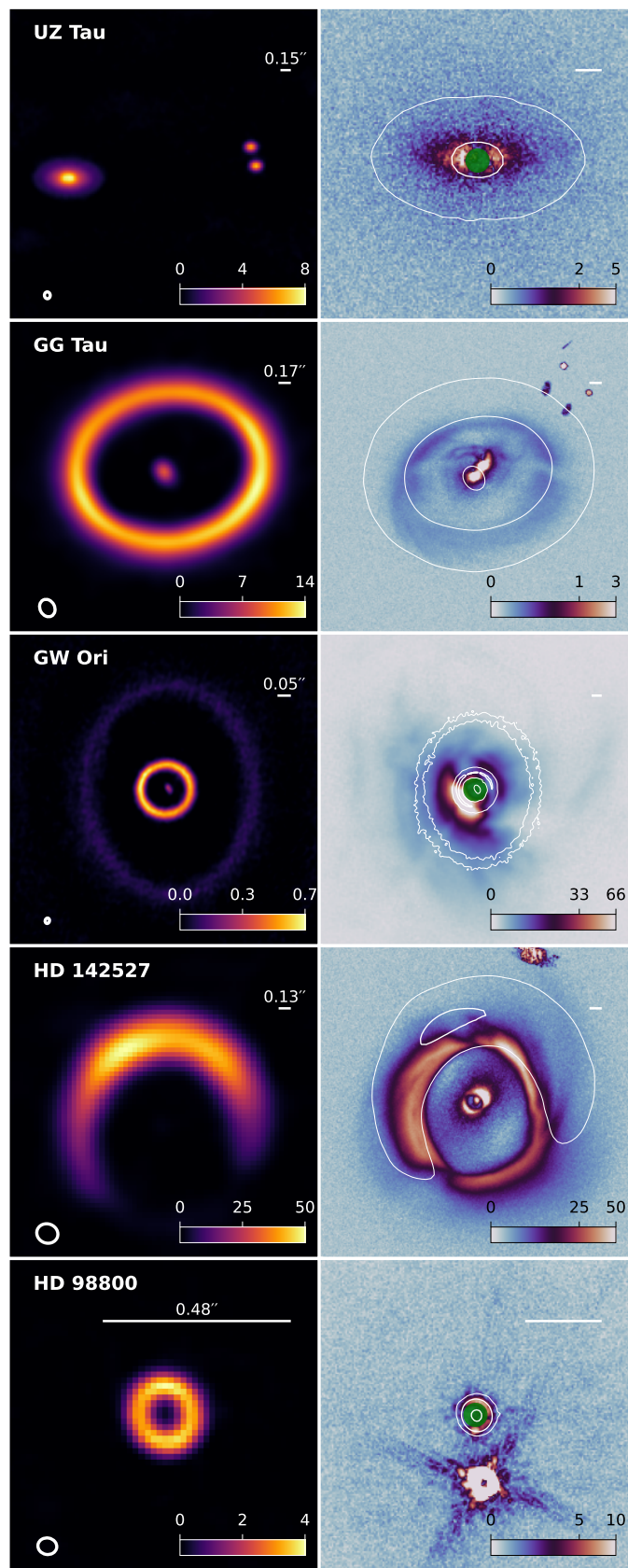


**Figure 4.** Gallery of circumbinary discs (CBDs) with internal companions, processed using the same procedure as described in Figure 3. The SPHERE data are taken at 1.65  $\mu\text{m}$ , except HD 142527 which was observed at 2.15  $\mu\text{m}$ . The colour scales have been adjusted to enhance the visibility of circumstellar extended emission.

**GW Ori.** The triple system GW Ori, with its three close stars, was first resolved by [100], with orbital parameters later refined by [144] and [145]. The inner binary, GW Ori AB, has a period of 242 days and a semi-major axis of  $\sim 1$  au, while GW Ori AB-C orbits with a period of approximately 8 years and a semi-major axis of  $\sim 8$  au. Interestingly, the two orbital planes are misaligned by  $\sim 14^\circ$  [101]. The GW Ori disc comprises three distinct rings, as revealed by scattered light and continuum observations [101,146]. The central regions are cleared of material by the stellar components, and all three rings are misaligned relative to the orbital planes of the stars, with the innermost ring further misaligned with the two outer rings. Modelling indicates that the observed disc tearing is driven by the gravitational torque from the inner triple star [101,135,147]. Despite significant progress in characterising this system, many questions remain about the specific physical processes that led to the current configuration.

**HD 142527.** The disc of HD 142527 features a large inner cavity observable in both NIR and millimetre wavelengths [148]. NIR observations also reveal central emission within the cavity, tracing material near the binary and casting shadows on the outer disc [103–105]. In addition to the cavity, the disc exhibits striking features likely caused by disc-binary interactions. These include large spiral arms near the cavity edge and in the outer disc [102,105,149], a bright horseshoe-shaped asymmetry in the northern disc [148], and fast flows connecting the inner and outer regions [150]. Initial models suggested a binary orbit with a semi-major axis  $a \lesssim 50$  au could account for these structures [28]. However, more recent measurements place the binary at  $a \sim 11$  au, insufficient to explain the observed features [151]. These discrepancies suggest the presence of additional physics or a hidden companion influencing the system [32]. Notably, the new orbital solution reveals a mutual inclination of  $\sim 8^\circ$  between the binary and the outer disc.

**HD 98800.** Located 45 pc away in the TW Hya association, HD 98800 is a  $\sim 10$  Myr-old quadruple system [152–154]. It consists of two close binaries, HD 98800 A and B, situated to the north and south of the system, respectively, with well-characterized orbits [155]. A small, tidally truncated disc around HD 98800 B has been resolved at 0.88 mm, with a narrow ring width of 2 au in dust emission and a central cavity in CO emission [107,156,157]. These features align closely with models of tidal truncation by both the inner and outer binaries [158,159]. Remarkably, the plane of the CBD is in a polar configuration relative to the orbit of HD 98800 B, making it the first known system of its kind [159]. With such unique configurations now observed and modelled, ongoing theoretical efforts aim to explore how planet formation proceeds in polar discs [160,161].

## 5. Open questions in the field

As showcased in previous sections, the interaction between multiple stellar systems and protoplanetary discs offers a rich field of study. Over the past two decades, significant progress has been made in understanding how stellar multiplicity shapes disc structures and evolution. Here, we synthesise recent efforts made to address the connection between stellar orbits and disc morphology, the dynamics of dust multiple stellar systems, and the broad implications for planet formation.

### 5.1. Linking stellar orbits to disc morphology

The orbital characteristics of companion stars, including eccentricity, inclination, and semi-major axis, play a pivotal role in determining disc morphology. Eccentric orbits, for example, enhance tidal torques, creating large asymmetries within discs. In circumbinary discs (CBDs), circular and eccentric binaries can carve elongated cavities and excite strong spiral density waves [11,12,32]. Meanwhile, circumstellar discs (CSDs) in eccentric systems often exhibit truncated outer edges and steeper surface density profiles, which can accelerate radial drift and affect the distribution of solids. Inclination is another critical factor, particularly in systems where the companion star's orbit is misaligned with the disc plane. Misaligned configurations induce precession and can lead to warped or even torn discs, as seen in simulations of systems like GW Ori [101,147]. These effects are not limited to

binaries; in hierarchical triples, such as GG Tau, interactions between the inner and outer stars further complicate the disc dynamics, potentially leading to distinctively warped or nested structures [27,34,141].

Recent observational campaigns have provided compelling evidence linking stellar orbits to disc features. In systems like HD 142527, HD 100453, and AB Aur, large-scale spiral arms and azimuthal asymmetries have been directly attributed to gravitational perturbations by stellar companions [28,29,162]. However, in some cases, the binary scenario alone does not fully account for the observed complexity of disc structures, and in others, the proposed stellar companions remain below current detection limits. On top of this, the observed misalignments in systems such as GW Ori further reinforce the connection between orbital dynamics and disc morphology. Figure 5 illustrates how hydrodynamical models of circumstellar discs replicate observed features such as spirals and precession while testing new dynamical scenarios. In this model, an inner gas giant planet (located at about 20 au) carves the inner disc cavity and efficiently drives the precession of the innermost regions, which are expected to cast shadows consistent with observations.

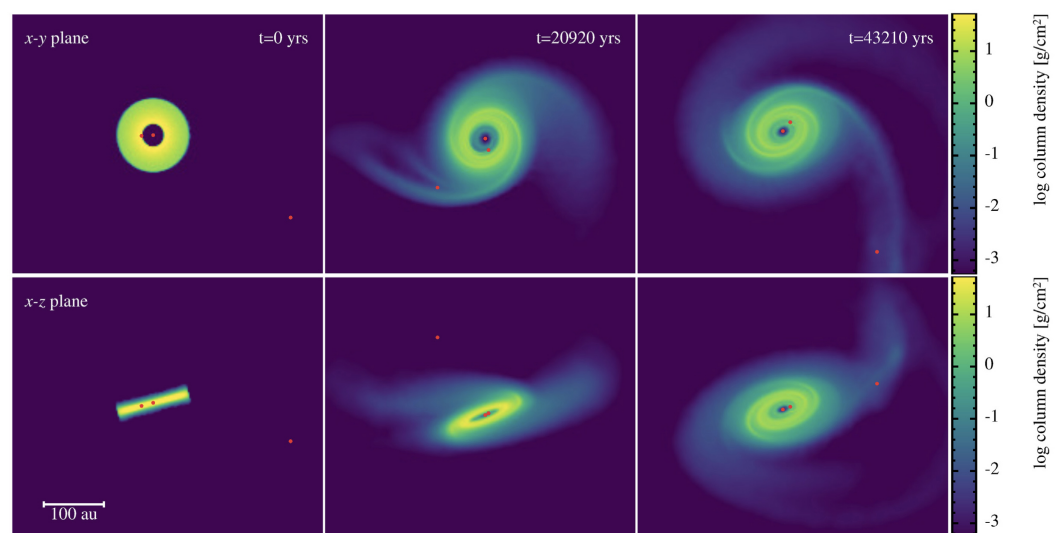


**Figure 5.** Column density rendering of a hydrodynamical model of the system HD 100453 including a central star, a disc with an inner companion of  $5 M_J$  at 20 au, and a misaligned external companion (star B) with the following parameters:  $q = 0.12$ ,  $a = 207$  au,  $e = 0.32$ ,  $i = 49^\circ$ ,  $\Omega = 47^\circ$ ,  $\omega = 18^\circ$ . The disc has an outer edge at 60 au and an aspect ratio  $H/R$  equal to 0.05. The top row shows the system in the plane of the sky, and the bottom row in a perpendicular plane. Stars and the planet are marked in red. Extended spirals and disc precession are driven by the external companion, while the inner planet carves a central cavity in the disc. Figure adapted from [130], with permission of the authors.

Triple stellar systems introduce additional complexity, carving intricate inner cavities in their discs and giving rise to diverse morphologies and kinematics. Detailed mapping, as in GG Tau, reveals how hierarchical arrangements shape accretion dynamics and structural features [68,97]. Material crossing the cavity from the circumtriple disc to the inner stars is influenced by stellar motion, leading to luminosity variability, with accretion bursts exhibiting varying periodicity based on the stellar orbits [30,163]. As shown in Figure 6, recent hydrodynamical simulations demonstrate how stellar multiplicity affects accretion by comparing a pure binary case against two similar configurations of triple systems: one where the secondary star is split into two stars, and another where the primary star is split into two stars [134]. In principle, measuring accurate individual mass accretion rates onto the stars could provide additional constraints on the orbital parameters of young multiple stellar systems. At a more general level, multi-wavelength observations and long-term monitoring are essential for disentangling the roles of stellar components, reconstructing their 3D geometry, and refining parameters through modelling [25,31,33,101,131].

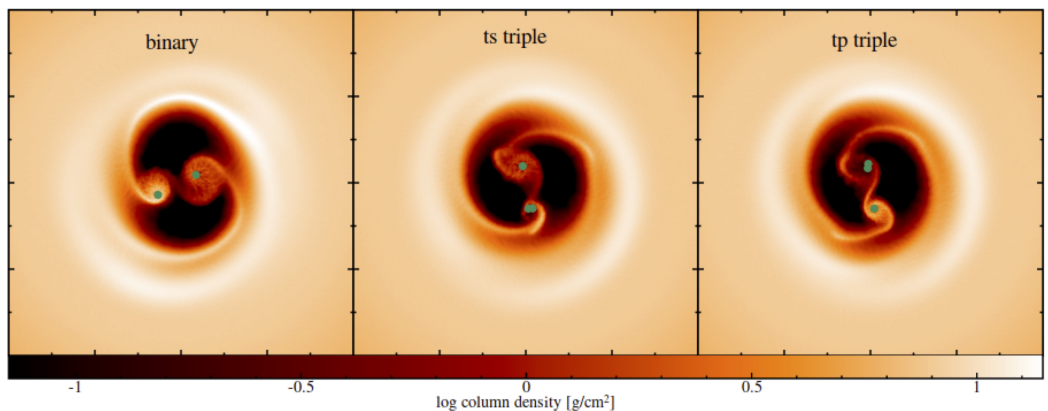


**Figure 6.** Snapshots of three high-resolution simulations showing the gas density. Green dots represent the stars. The first column depicts the pure binary case, the central column shows a triple system obtained by splitting the secondary star of the binary (type ts), and the rightmost column shows a triple system obtained by splitting the primary star of the binary (type tp). These simulations evolved over 55 orbits of the outer binary. Figure adapted from [134], with permission of the authors.

### 5.2. Dust dynamics and growth in multiple stellar systems

In multiple stellar systems, the dynamics of gas and dust are significantly influenced by the gravitational forces of nearby stellar companions. These tidal forces shape the overall structure of the protoplanetary disc, affecting the spatial distribution and evolution of gas and solids. Dust discs, in particular, are typically more compact than their gaseous counterparts due to the effects of radial drift [51,57]. This process is particularly pronounced in CSDs, where the steep radial surface density profile of gas accelerates the inward drift of solids. As a result, dust grains are expected to be rapidly accreted onto the central star unless the local solid density becomes sufficiently high to trigger dust instabilities. One potential mechanism for halting this drift is the formation of self-induced dust traps [164], which can play a critical role in preventing dust loss in circumstellar discs within binary systems, thereby fostering favourable conditions to planet formation.

In CBDs, solids evolve differently: dust is expected to accumulate near the inner CBD edge, where tidal interactions with the binary companion create strong radial and azimuthal pressure gradients [e.g. 20]. These pressure maxima serve as natural dust traps, facilitating the growth of larger solids [21,165,166]. Misaligned or eccentric CBDs introduce further complexity, as they are particularly efficient at capturing large dust particles. For instance, differences in the precession rates of gas and dust in misaligned CBDs can result in the formation of dust rings [167], which have been recently extended to polar configurations [161,168,169]. Similarly, warped discs can induce oscillatory gas motions, creating high-density dust concentrations on dynamical timescales [170]. These dust trapping mechanisms, driven by gravitational perturbations, are critical for understanding the emergence of planets within CBDs, particularly in their inner regions. However, the intricate interplay of these processes remains to be fully explored.

The presence of nearby stellar companions also poses challenges for dust growth by exciting high collisional velocities between dust grains. At such velocities, collisions are more likely to result in fragmentation than in coagulation [171], potentially hindering the formation of larger particles. Yet, the very same perturbers imprint high-density structures in the disc, such as spirals, warps, and crescent-shaped asymmetries, as discussed in Sections 3.2 and 4.2. These features could serve as efficient dust traps, potentially fostering grain growth within localized regions. Despite advances in understanding, the competition between fragmentation and growth remains poorly constrained in multiple stellar systems. High-resolution observations, laboratory experiments, and sophisticated numerical simulations are required to disentangle the effects of perturbations from the intrinsic growth processes of dust particles.

In this context, the advent of ALMA has revolutionised the study of dust properties in protoplanetary discs, offering unprecedented resolution and sensitivity. A widely used method for characterizing grain properties involves fitting a dust model to the system's spectral energy distribution (SED), enabling insights into grain size distributions and compositions regardless of the stellar multiplicity [e.g. 172]. Scattered light imaging in the near-infrared (NIR) provides complementary constraints on grain properties, but its applicability is limited in discs with non-axisymmetric structures [e.g. 173]. In the millimetre regime, fitting the SED slope across multiple wavelengths has emerged as a robust technique for probing grain size variations within discs. Resolved observations, often radially or azimuthally averaged to reduce computational costs, allow for the spatial modelling of grain properties [e.g. 174,175]. Systematic studies applying these methods have begun to characterise dust populations in multiple stellar systems [176,177]. Intriguingly, [177] found no correlation between the presence of multiple stars and the maximum grain size in their sample. Similarly, [178] detected no signs of dust growth at the location of a continuum over-density in AB Aur, while [176] concluded that grain growth in the outer regions of discs is often constrained by the fragmentation barrier [179]. Remarkably, new methods are emerging to better characterise azimuthal asymmetries in protoplanetary discs [e.g. 180], which are highly relevant for multiple stellar systems [e.g. 136]. Overall, a larger sample is required to be able to assess the influence of stellar multiplicity on dust growth.

Numerical simulations offer critical insights into the growth and evolution of dust grains, though they often come at the expense of high spatial resolution. For example, 1D simulations can accurately model multiple dust populations, incorporating collisions between grains of varying sizes and porosity evolution [e.g. 181]. However, the introduction of multiple stars breaks the symmetry of the problem, necessitating a multi-dimensional approach. Recent advances in 3D simulations have enabled the inclusion of dust size and porosity evolution in single stellar systems, though inter-grain collisions are typically limited to particles of similar sizes [182,183]. These simulations have shown that particle growth to decimetre scales requires porosity and compaction over time, typically within the snowline, where fragmentation velocities are higher. In multiple stellar systems, 3D hydrodynamical simulations with live radiative transfer indicate that snowlines tend to align with the cavity edges of CBDs [184,185]. This alignment implies that significant dust growth is constrained to the inner regions of CBDs where conditions are more favourable for planetesimal formation.

### 5.3. Implications for planet formation

The modified evolutionary pathways of discs in multiple stellar systems, eventually impact the formation of planetesimals and hence the resulting planetary architectures. In such systems, disc truncation by stellar companions limits the available mass for planet formation while concentrating material in smaller, high-density regions. For instance, the concentration of solids near the cavity edges of CSDs and CBDs could explain the population of short-period exoplanets in binaries ([https://exoplanet.eu/planets\\_binary/](https://exoplanet.eu/planets_binary/)). If confirmed, this trend would reinforce the role of stellar multiplicity in shaping exoplanet diversity. On top of this, the presence of strong tidal interactions in multiple systems could also influence planetary migration pathways [e.g. 186]. This formation scenario may favour the formation of rocky, terrestrial planets over gas giants, contrasting with the broader diversity of planetary types seen in single stellar systems [e.g. 187].

Moreover, misaligned discs constitute unique planetary factories for producing unconventional orbital configurations. In fact, simulations and observations suggest that such systems, especially polar CBDs, could host planets on highly inclined, eccentric, or even retrograde orbits [e.g. 16,188,189]. These planetary outcomes reflect the early gravitational influence of stellar companions on the disc and highlight how multiplicity drives diversity in exoplanetary architectures. For example, the inclined planetary orbits observed in systems like TOI-1338/BEBOP-1 (b and c) serve as valuable test beds for studying planet

formation around binary stars [190]. In the near future, the continued progress of surveys is expected to reveal additional multi-planetary architectures.

However, the structural and dynamical complexity of discs in multiple stellar systems poses significant challenges for detecting and characterising exoplanets. Techniques such as astrometry, transits, and radial velocity suffer from noise and systematic effects introduced by stellar companions. Despite these challenges, the emerging understanding of disc dynamics and their influence on planet formation can directly inform observational strategies. For example, high-precision astrometric missions like *Gaia* [108,191,192] and advanced radial velocity surveys like BEBOP [193] now offer improved sensitivity to planets in these complex environments. The upcoming search will be crucial to better understand the planet occurrence rate and the differences with respect to single stellar systems [194–196].

## 6. Discussion and conclusions

In this review, we have highlighted the profound impact of stellar multiplicity on the dynamics, structure, and evolution of protoplanetary discs — demonstrating how their interplay offers unique insights into the complex processes of planet formation. We summarise our main conclusions and future developments as follows:

- **Stellar multiplicity shapes disc structures and planet formation.** The presence of multiple stars significantly alters the dynamics and morphology of protoplanetary discs, leading to truncation, misalignment, and dust traps. These structures influence where and how planetesimals form, potentially favouring rocky planets due to limited mass reservoirs for gas giant formation.
- **Misaligned and polar discs produce unique planetary architectures.** Misaligned and polar circumbinary discs drive the formation of planets with unconventional orbital configurations, such as inclined, eccentric, or retrograde orbits. These configurations exemplify the diversity of planetary outcomes shaped by stellar multiplicity.
- **The observation of exoplanets in multiple systems remains challenging,** mainly due to noise and systematic effects from stellar companions. This is one of the current bottlenecks in the field. However, advances in astrometry (e.g., *Gaia* [108]), radial velocity surveys (e.g., BEBOP [193]), and high-resolution imaging are beginning to address these challenges, enabling exploration of this under-sampled population.

Future research on stellar multiplicity and its influence on planet formation will require a coordinated effort combining high-resolution observations with advanced numerical modelling. Instruments such as the James Webb Space Telescope (JWST) and ALMA together with the next generation of Extremely Large Telescopes (ELTs) and Square Kilometre Array (SKA) will provide critical constraints regarding the structure and dynamics of protoplanetary discs, particularly in their inner regions where planets actively form. When paired with 3D hydrodynamical simulations incorporating realistic treatments of dust growth, fragmentation, and companion-induced perturbations, these efforts will deepen our understanding of planet formation in multiple stellar systems.

Expanding the observational sample of discs in multiple stellar systems (see our extended list in Appendix B) will also help establish statistical links between stellar configurations, disc properties, and emerging planetary architectures. This will clarify the role of stellar multiplicity in shaping planetary diversity, particularly in systems with polar or misaligned discs, which may offer unique pathways for planet formation. These efforts will guide the development of targeted strategies to detect and characterise exoplanets in multiple stellar systems — a crucial step toward understanding the full spectrum of planetary outcomes across all stellar environments.

To conclude on a historical note, we would like to quote Sir William Herschel, a pioneering figure in astronomy and the study of multiple stellar systems, who in 1789 wrote: *"This method of viewing the heavens seems to throw them into a new kind of light. They now are seen to resemble a luxuriant garden, which contains the greatest variety of productions, in different flourishing beds; and one advantage we may at least reap from it is, that we can, as it were, extend the range of our experience to an immense duration".*

**Author Contributions:** Conceptualization, N.C., A.A, P.P.; methodology, N.C., A.A, P.P.; software, A.A.; data curation, A.A, N.C.; writing—original draft preparation, N.C., A.A, P.P.; writing—review and editing, N.C., A.A; visualization, A.A.; supervision, N.C.; project administration, N.C.; funding acquisition, N.C. All authors have read and agreed to the published version of the manuscript.

**Funding:** This project has received funding from the European Research Council (ERC) under the European Union Horizon Europe programme (grant agreement No. 101042275, project Stellar-MADE).

**Institutional Review Board Statement:** Not applicable.

**Data Availability Statement:** The SPHERE observational data used in this study have been downloaded from the ESO Science Archive Facility using the following queries :

- [HT Lup](#),
- [S CrA](#),
- [UY Aur](#),
- [T Tau](#),
- [HD 100453](#),
- [UZ Tau](#),
- [GG Tau](#),
- [GW Ori](#),
- [HD 142527](#),
- [HD 98800](#).

These raw data were reduced and processed using the publicly available [IRDAP pipeline](#).

The ALMA data used in this work were downloaded from the ALMA archive using the available data products from the following project codes :

- HT Lup: 2016.1.00484.L [[82](#)],
- S CrA: 2019.1.01792.S,
- UY Aur: 2016.1.01164.S,
- T Tau: 2019.1.00703.S,
- HD 100453: 2017.1.01678.S,
- UZ Tau: 2016.1.01164.S,
- GG Tau: 2018.1.00532.S,
- GW Ori: 2018.1.00813.S,
- HD 142527: 2015.1.01353.S,
- HD 98800: 2017.1.00350.S.

**Acknowledgments:** This research has made use of the Astrophysics Data System, funded by NASA under Cooperative Agreement 80NSSC21M00561. This paper makes use of the following ALMA data: ADS/JAO.ALMA#2017.1.01678.S, 2019.1.00703.S, 2016.1.00484.L, 2016.1.01164.S, 2016.1.01164.S, 2019.1.01792.S, 2015.1.01353.S, 2018.1.00532.S, 2018.1.00813.S, and 2017.1.00350.S. ALMA is a partnership of ESO (representing its member states), NSF (USA) and NINS (Japan), together with NRC (Canada), NSC and ASIAA (Taiwan), and KASI (Republic of Korea), in cooperation with the Republic of Chile. The Joint ALMA Observatory is operated by ESO, AUI/NRAO and NAOJ. We thank Martina Toscani, Ulko, and the entire Stellar-MADE team for their support during this project.

**Conflicts of Interest:** The authors declare no conflicts of interest. The funders had no role in the design of the study; in the collection, analyses, or interpretation of data; in the writing of the manuscript; or in the decision to publish the results.

## Abbreviations

The following abbreviations are used in this manuscript:

CBD	Circumbinary Disc
CSD	Circumstellar Disc
CTD	Circumtriple Disc
ALMA	Atacama Large Millimeter Array
SPHERE	Spectro-Polarimetric High-Contrast Exoplanet Research
VLA	Karl G. Jansky Very Large Array
VLT	Very Large Telescope
NIR	Near Infrared

### Appendix A. Orbital parameters

Here, we list the relevant orbital parameters, along with their definitions, which are key for describing binary orbits [197]. These parameters are illustrated in Fig. 2.

1. The semi-major axis ( $a$ ), which represents the average distance between the star and the system's centre of mass. It is an indicator of the orbit's size and, by extension, the stellar orbital period around the common centre of mass. For a binary system with masses  $m_1$  and  $m_2$ , this can be obtained as follows:

$$T = 2\pi \sqrt{\frac{a^3}{G(m_1 + m_2)}}, \quad (\text{A1})$$

where  $G$  is the gravitational constant. It is however common to work with the orbital frequency  $\Omega_k = 2\pi/T$ .

2. The eccentricity ( $e$ ) describes the shape of the orbit. A value of 0 corresponds to a perfectly circular orbit, while values approaching 1 indicate highly elliptical orbits. Eccentricity influences the variation in distance between the two bodies during their motion. The closest and farthest points along the orbit are known as the periapsis and apoapsis, respectively, given by  $r_{\min} = a(1 - e)$  and  $r_{\max} = a(1 + e)$ .
3. The inclination ( $i$ ) measures the angle between the orbital plane and the reference plane, typically the plane of the sky. This parameter is critical for understanding the orbital orientation relative to the observer's line of sight.
4. The longitude of the ascending node ( $\Omega$ ) represents the point on the orbit where the star crosses the reference plane moving from South to North (towards the  $\Upsilon$  sign in Figure 2). This parameter is essential for determining the orbit's orientation in space.
5. The argument of periapsis ( $\omega$ ) specifies the orbital orientation of the ellipse within its plane. It defines the angular position of the periapsis relative to the ascending node.
6. The true anomaly ( $\nu$ ) is the angle between the direction of the periapsis and the star's current position. Alternatively, the mean anomaly ( $M$ ) provides a convenient way to represent the orbital angle between the periapsis and the star's position. It accounts for Kepler's second law by defining angles such that each successive segment encloses equal areas within the elliptical orbit, corresponding to equal time intervals.

### Appendix B. List of young multiple stellar systems with protoplanetary discs

Below, we provide an extensive (although not exhaustive) list of multiple stellar systems of interest with protoplanetary discs. The latter can either be circumstellar (CSD), circumbinary (CBD), or circumtriple (CTD).

**Table B1.** List of multiple stellar systems with protoplanetary discs.

Name	RA (hh:mm:ss)	Dec (dd:mm:ss)	Number of stars	Type of disc(s) <sup>1</sup>	References
99 Her	18:07:01.591	+30:33:43.58	2	CBD	[198]
AK Sco	16:54:44.849	-36:53:18.57	2	CBD	[199]
AS 205 <sup>2</sup>	16:11:31.346	-18:38:25.96	3	CSD, CBD	[200–202]

**Table B1.** continued.

Name	RA (hh:mm:ss)	Dec (dd:mm:ss)	Number of stars	Type of disc(s)	References
BF Ori	05:37:13.262	-06:35:0.57	2	CSD	[203,204]
BHB2007 11	17:11:23.178	-27:24:31.53	2	CSD,CBD	[205]
Bernhard 2	07:14:45.39	-09:01:52.10	2	CBD	[206,207]
CD22 11432	16:14:11.070	-23:05:36.07	2	CSD/CBD	[208–211]
CHX 22	11:12:42.671	-77:22:22.94	2	CBD	[212]
CIDA 9	05:05:22.86	+25:31:31.2	2	CSD	[213,214]
CQ Tau	05:35:58.467	+24:44:54.09	2	CSD	[204,215]
CS Cha	11:02:24.876	-77:33:35.67	2	CBD	[216,217]
CoKu Tau/4	04:41:16.810	+28:40:00.0738	2	CBD	[218,219]
CoRoT 2239	06:41:44.22	+09:25:02.398	2	CBD	[220]
DD Tau	04:18:31.129	+28:16:29.15	2	CSD	[221]
DF Tau	04:27:2.793	+25:42:22.45	2	CSD	[87,222]
DH Tau	04:29:41.659	26:32:56.508	2	CSD	[223]
DK Tau	04:30:44.243	+26:01:24.65	2	CSD	[214]
DQ Tau	04:46:53.058	+17:00:00.14	2	CBD	[224,225]
DoAr 43	16:31:30.882	-24:24:39.888	2	CSD	[226,227]
DoAr 51	16:32:11.795	-24:40:21.64	2	CSD	[226,227]
EDJ2009-156	03:28:51.029	+31:18:18.409	2	CSD	[228,229]
EDJ2009-183	03:28:59.297	+31:15:48.410	2	CSD	[228,229]
EDJ2009-269	03:30:44.014	+30:32:46.812	2	CSD	[228,229]
FO Tau	04:14:49.284	+28:12:30.51	2	CSD	[52,87]
FQ Tau	04:19:12.813	+28:29:32.98	2	CSD	[52]
FU Ori <sup>2</sup>	05:45:22.365	+09:04:12.29	2	CSD	[230,231]
FU Tau	04:23:35.738	25:02:59.633	2	CSD	[223]
FV Tau	04:26:53.537	+26:06:54.28	4	CSD	[214]
FX Tau	04:30:29.618	+24:26:45.03	2	CSD	[214]
FZ Tau	04:32:31.764	24:20:03.000	2	CSD	[223]
GG Tau	04:32:30.351	+17:31:40.49	5	CSD,CTD	[91–97]
GSS 31	16:26:23.368	-24:20:59.579	2	CSD	[226,227]
GV Tau	04:29:23.731	+24:33:00.22	3	CSD,CBD	[225,232,233]
GW Ori	05:29:08.393	+11:52:12.67	3	CBD,CTD	[98–101]
HBC 387	04:26:54.401	+26:06:50.95	2	CSD	[214]
HBC 411	04:35:40.938	+24:11:8.49	2	CSD	[214]
HBC 494	05:40:27.450	-07:27:30.06	2	CSD	[234]
HD 100453	11:33:05.577	-54:19:28.55	2	CSD	[88,89]
HD 104237	12:00:05.087	-78:11:34.57	2	CBD	[235,236]

**Table B1.** continued.

Name	RA (hh:mm:ss)	Dec (dd:mm:ss)	Number of stars	Type of disc(s)	References
HD 106906	12:17:53.192	-55:58:31.89	2	CBD	[237,238]
HD 131511	14:53:23.765	+19:09:10.07	2	CBD	[239]
HD 141569	15:49:57.748	-03:55:16.34	3	CSD	[204,240]
HD 142527	15:56:41.888	-42:19:23.25	2	CSD,CBD	[102–105]
HD 144432	16:06:57.953	-27:43:9.76	3	CSD	[241,242]
HD 150193	16:40:17.924	-23:53:45.19	2	CSD	[204,243]
HD 200775	21:01:36.921	+68:09:47.79	3	CBD	[244–246]
HD 34700	05:19:41.409	+05:38:42.78	3	CBD	[247,248]
HD 36112	05:30:27.529	+25:19:57.08	2	CSD	[204,249]
HD 37258	05:36:59.250	-06:09:16.33	2	CSD	[203,204]
HD 98800	11:22:05.290	-24:46:39.76	4	CBD	[106,107]
HH 250	19:21:13.675	+10:52:31.00	2	CSD,CBD	[250]
HH 48	11:04:22.800	-77:18:07.99	2	CSD	[251]
HK Ori	05:31:28.050	+12:09:10.30	3	CSD	[204,215]
HK Tau	04:31:50.572	+24:24:17.78	2	CSD	[252]
HN Tau	04:33:39.363	+17:51:52.29	2	CSD	[52]
HP Cha	11:08:15.216	-77:33:53.17	3	CSD, CBD	[212,253]
HT Lup	15:45:12.868	-34:17:30.64	3	CSD	[81,82]
HV Tau <sup>2</sup>	04:38:35.290	+26:10:38.64	3	CSD	[254,255]
Haro 6-37	04:46:59.078	17:02:39.670	2	CSD	[223]
Hn 23	13:04:24.060	-76:50:01.390	2	CSD	[223]
IC348 LRL31	03:44:18.17	+32:04:57.00	2	CBD	[256,257]
IC348 MMS	03:43:57.065	+32:03:04.788	3	CSD	[229,258]
IRAS 03282+3035	03:31:20.939	+30:45:30.273	2	CSD	[229,258]
IRAS 03282+30355	03:44:43.298	+32:01:31.236	3	CSD	[229,258]
IRAS 03292+3039	03:32:17.928	+30:49:47.825	2	CSD	[229,258]
IRAS 03292+30392	03:25:22.409	+30:45:13.258	2	CSD	[229,258]
IRAS 04125+2902	04:15:42.787	+29:09:59.83	2	CSD	[259]
IRAS 04158+2805	04:18:58.134	+28:12:23.36	2	CSD,CBD	[24,40,260]
IRAS 04298+2246	04:32:49.117	+22:53:2.85	4	CSD	[214]
IRAS 16293-2422	16:32:22.560	-24:28:31.80	3	CSD,CBD	[261,262]
IRAS 17216-3801	17:25:6.517	-38:04:0.44	2	CSD,CBD	[263]
IRAS F13052-7653N	13:09:10.980	-77:09:44.140	2	CSD	[223]
IRS 43	16:27:26.950	-24:40:50.500	2	CSD,CBD	[264,265]
ISO-Oph 2 <sup>2</sup>	16:25:38.127	-24:22:36.19	3	CSD	[266]
IT Tau	04:33:54.701	+26:13:27.52	2	CSD	[52]

**Table B1.** continued.

Name	RA (hh:mm:ss)	Dec (dd:mm:ss)	Number of stars	Type of disc(s)	References
J10555973-7724399	10:55:59.731	-77:24:39.913	2	CSD	[223]
J10574219-7659356	10:57:42.200	-76:59:35.664	2	CSD	[223]
J10581677-7717170	10:58:16.774	-77:17:17.056	2	CSD	[223]
J11023265-7729129	11:02:32.654	-77:29:12.977	2	CSD	[267]
J11040909-7627193	11:04:09.090	-76:27:19.379	2	CSD	[223]
J11072074-7738073	11:07:20.744	-77:38:07.354	3	CSD	[223]
J11072825-7652118	11:07:28.256	-76:52:11.899	2	CSD	[267]
J11075792-7738449	11:07:57.928	-77:38:44.927	2	CSD	[223]
J11080002-7717304	11:08:00.025	-77:17:30.484	2	CSD	[267]
J11080148-7742288	11:08:01.486	-77:42:28.854	2	CSD	[223]
J11080297-7738425	11:08:02.975	-77:38:42.590	2	CSD	[223]
J11091812-7630292	11:09:18.129	-76:30:29.250	2	CSD	[267]
J11095340-7634255	11:09:53.405	-76:34:25.511	2	CBD	[223]
J11095407-7629253	11:09:54.076	-76:29:25.310	2	CSD	[223]
J11095873-7737088	11:09:58.738	-77:37:08.879	2	CSD	[223]
J11100010-7634578	11:10:00.108	-76:34:57.893	2	CBD	[223]
J11100704-7629376	11:10:07.045	-76:29:37.698	2	CSD	[223]
J11103801-7732399	11:10:38.018	-77:32:39.905	2	CSD	[223]
J11105597-7645325	11:10:55.974	-76:45:32.573	2	CSD	[223]
J11122441-7637064	11:12:24.415	-76:37:06.406	2	CSD	[267]
J11175211-7629392	11:17:52.117	-76:29:39.264	2	CSD	[223]
J15354856-2958551	15:35:48.565	-29:58:55.182	2	CSD	[210]
J15534211-2049282	15:53:42.119	-20:49:28.218	3	CSD	[210]
J16001844-2230114	16:00:18.441	-22:30:11.488	2	CSD	[210]
J16014086-2258103	16:01:40.869	-22:58:10.384	2	CSD	[210]
J16062196-1928445	16:06:21.963	-19:28:44.566	2	CSD	[268]
J16082751-1949047	16:08:27.520	-19:49:04.721	2	CSD	[268]
J16083070-3828268	16:08:30.687	-38:28:27.280	2	CSD	[269,270]
J16084940-3905393	16:08:49.382	-39:05:39.825	2	CSD	[269,270]
J16085373-3914367	16:08:53.725	-39:14:37.170	2	CSD	[223]
J16095628-3859518	16:09:56.281	-38:59:51.973	3	CSD	[269,270]
J16101984-3836065	16:10:19.840	-38:36:06.800	2	CSD	[223]
J16133650-2503473	16:13:36.510	-25:03:47.340	2	CSD	[210]
J16135434-2320342	16:13:54.347	-23:20:34.253	2	CSD	[210]
KH15D <sup>3</sup>	06:41:10.340	+09:28:33.49	2	CBD	[271-273]
KK Oph	17:10:8.110	-27:15:19.01	2	CSD	[203,274]

**Table B1.** continued.

Name	RA (hh:mm:ss)	Dec (dd:mm:ss)	Number of stars	Type of disc(s)	References
L1448 IRS1	03:25:09.449	+30:46:21.933	2	CSD	[229]
L1448 IRS3	03:25:36.379	+30:45:14.728	6	CSD,CBD	[229]
L1455-FIR2	03:27:38.268	+30:13:58.448	2	CSD	[229,258]
L1551 IRS5	04:31:34.169	+18:08:4.269	2	CBD	[275–277]
L1689 IRS5	16:31:52.11	-24:56:15.7	3	CSD	[226,227]
MHO2	04:14:26.401	+28:05:59.64	3	CBD	[278,279]
NGC1333 IRAS1	03:28:37.090	+31:13:30.788	2	CSD	[229,258]
NGC1333 IRAS2	03:28:55.569	+31:14:37.025	4	CSD	[229,258,280]
NGC1333 IRAS4	03:29:10.537	+31:13:30.933	4	CSD	[229,258]
NGC1333 IRAS7	03:29:11.258	+31:18:31.073	5	CSD	[229,258]
Per-emb-17	03:27:39.105	+30:13:03.068	2	CSD	[229,258]
Per-emb-40	03:33:16.669	+31:07:54.901	2	CSD	[229,258]
ROXs 42C	16:31:15.745	-24:34:2.16	3	CBD	[200,281–283]
ROph 36	16:33:55.615	-24:42:05.002	2	CBD	[227,256]
RW Aur <sup>2</sup>	05:07:49.566	+30:24:5.18	2	CSD	[284,285]
R CrA	19:01:53.676	-36:57:08.30	2	CBD	[286,287]
SR 24 <sup>2</sup>	16:26:58.425	-24:45:46.34	3	CSD,CBD	[288–290]
SR 9	16:27:40.29	-24:22:04.0	2	CSD	[226,227]
SVS 13	03:29:03.764	+31:16:03.808	5	CSD,CBD	[229,258]
SV Cep	22:21:33.217	+73:40:27.10	2	CSD	[204,249]
S CrA	19:01:08.597	-36:57:19.90	2	CSD	[83,84]
Sz 123	16:10:51.310	-38:53:12.800	2	CSD	[269,270]
Sz 65	15:39:27.772	-34:46:17.21	2	CSD	[291]
Sz 74	15:48:05.213	-35:15:53.342	2	CSD	[269,270]
Sz 75	15:49:12.086	-35:39:05.463	2	CSD	[270,292]
Sz 77	15:51:46.941	-35:56:44.531	2	CSD	[270,292]
Sz 81	15:55:50.264	-38:01:34.087	2	CSD	[269,270]
Sz 88	16:07:00.582	-39:02:19.913	3	CSD	[269,270]
TMC 1	04:41:45.900	+25:41:26.99	2	CSD	[293]
TWA3A	11:10:27.894	-37:31:51.97	3	CBD	[294,295]
T Tau	04:21:59.432	+19:32:06.43	3	CSD,CBD	[87]
UX Tau <sup>2</sup>	04:30:3.996	+18:13:49.44	4	CSD	[288,296,297]
UY Aur	04:51:47.389	+30:47:13.55	2	CSD	[85,86]
UZ Tau	04:32:43.022	+25:52:30.90	4	CSD,CBD	[87,90]
V1685 Cyg	20:20:28.241	+41:21:51.53	2	CSD	[204,298]
V347 Aur	04:56:57.022	+51:30:50.88	2	CBD	[299]

**Table B1.** continued.

Name	RA (hh:mm:ss)	Dec (dd:mm:ss)	Number of stars	Type of disc(s)	References
V4046 Sgr	18:14:10.482	-32:47:34.52	2	CBD	[300,301]
V710 Tau	04:31:57.798	+18:21:36.94	3	CSD	[214]
V773 Tau <sup>3</sup>	04:14:12.926	+28:12:12.36	4	CSD	[200,302–304]
V853 Oph	16:28:45.277	-24:28:18.91	3	CBD	[226,227]
V856 Sco	16:08:34.287	-39:06:18.33	2	CSD	[270]
V892 Tau	04:18:40.616	+28:19:15.63	3	CBD	[204,305,306]
V935 Sco	16:22:18.533	-23:21:48.15	2	CBD	[227,256]
VLA 1623	16:26:26.390	-24:24:30.80	4	CSD,CBD	[307,308]
WL4	16:27:18.487	-24:29:05.91	3	CBD	[226,309]
WL 20	16:27:15.698	-24:38:43.44	4	CSD,CBD	[310,311]
WSB 19	16:25:02.2	-24:59:31.0	2	CSD	[226,227]
WSB 38	16:26:46.429	-24:12:00.079	3	CSD	[226,227]
WSB 40	16:26:48.659	-23:56:34.14	2	CBD	[227,256]
WSB 74	16:31:54.747	-25:03:24.09	2	CBD	[227,312]
XY Per	03:49:36.337	+38:58:55.55	2	CSD	[249]
YLW 16	16:27:28.000	-24:39:30.00	3	CBD	[313,314]
Z CMa <sup>2</sup>	07:03:43.160	-11:33:06.21	2	CSD	[315]
alpha CrB	15:34:41.268	+26:42:52.87	2	CBD	[198]
beta Tri	02:09:32.627	+34:59:14.27	2	CBD	[198]

The sample includes systems found in the literature with at least two confirmed stars separated by less than 1000 au and with at least one disc that has been imaged. This table will be available in a machine-readable format. This table may not be exhaustive. We encourage the community to share any additional systems or updated information to help complete this dataset. Contributions can be directed to the corresponding authors of this work.

<sup>1</sup> CSD : CircumStellar Disc, CBD : CircumBinary Disc, CTD : CircumTriple Disc.

<sup>2</sup> System with an ongoing flyby event suspected, see [63] for more details.

<sup>3</sup> Disc inferred via eclipse events.

## References

- Manara, C.F.; Ansdel, M.; Rosotti, G.P.; Hughes, A.M.; Armitage, P.J.; Lodato, G.; Williams, J.P. Demographics of Young Stars and their Protoplanetary Disks: Lessons Learned on Disk Evolution and its Connection to Planet Formation. In Proceedings of the Protostars and Planets VII; Inutsuka, S.; Aikawa, Y.; Muto, T.; Tomida, K.; Tamura, M., Eds., July 2023, Vol. 534, *Astronomical Society of the Pacific Conference Series*, p. 539, [arXiv:astro-ph.SR/2203.09930]. <https://doi.org/10.48550/arXiv.2203.09930>.
- Armitage, P.J. *Astrophysics of planet formation, Second Edition*; 2020.
- Drażkowska, J.; Bitsch, B.; Lambrechts, M.; Mulders, G.D.; Harsono, D.; Vazan, A.; Liu, B.; Ormel, C.W.; Kretke, K.; Morbidelli, A. Planet Formation Theory in the Era of ALMA and Kepler: from Pebbles to Exoplanets. In Proceedings of the Protostars and Planets VII; Inutsuka, S.; Aikawa, Y.; Muto, T.; Tomida, K.; Tamura, M., Eds., July 2023, Vol. 534, *Astronomical Society of the Pacific Conference Series*, p. 717, [arXiv:astro-ph.EP/2203.09759]. <https://doi.org/10.48550/arXiv.2203.09759>.
- Offner, S.S.R.; Moe, M.; Kratter, K.M.; Sadavoy, S.I.; Jensen, E.L.N.; Tobin, J.J. The Origin and Evolution of Multiple Star Systems. In Proceedings of the Protostars and Planets VII; Inutsuka, S.; Aikawa, Y.; Muto, T.; Tomida, K.; Tamura, M., Eds., July 2023, Vol. 534, *Astronomical Society of the Pacific Conference Series*, p. 275, [arXiv:astro-ph.SR/2203.10066]. <https://doi.org/10.48550/arXiv.2203.10066>.
- Duchêne, G.; Kraus, A. Stellar Multiplicity. *ARA&A* **2013**, *51*, 269–310, [arXiv:astro-ph.SR/1303.3028]. <https://doi.org/10.1146/annurev-astro-081710-102602>.

6. Reipurth, B.; Clarke, C.J.; Boss, A.P.; Goodwin, S.P.; Rodríguez, L.F.; Stassun, K.G.; Tokovinin, A.; Zinnecker, H. Multiplicity in Early Stellar Evolution. In Proceedings of the Protostars and Planets VI; Beuther, H.; Klessen, R.S.; Dullemond, C.P.; Henning, T., Eds., January 2014, pp. 267–290, [arXiv:astro-ph.SR/1403.1907]. [https://doi.org/10.2458/azu\\_uapress\\_9780816531240-ch012](https://doi.org/10.2458/azu_uapress_9780816531240-ch012).
7. Bate, M.R. On the diversity and statistical properties of protostellar discs. *MNRAS* **2018**, *475*, 5618–5658, [arXiv:astro-ph.SR/1801.07721]. <https://doi.org/10.1093/mnras/sty169>.
8. Tokovinin, A. Architecture of Hierarchical Stellar Systems and Their Formation. *Universe* **2021**, *7*, 352, [arXiv:astro-ph.SR/2109.09118]. <https://doi.org/10.3390/universe7090352>.
9. Paczynski, B. A model of accretion disks in close binaries. *ApJ* **1977**, *216*, 822–826. <https://doi.org/10.1086/155526>.
10. Miranda, R.; Lai, D. Tidal truncation of inclined circumstellar and circumbinary discs in young stellar binaries. *MNRAS* **2015**, *452*, 2396–2409, [arXiv:astro-ph.EP/1504.02917]. <https://doi.org/10.1093/mnras/stv1450>.
11. Artymowicz, P.; Lubow, S.H. Dynamics of Binary-Disk Interaction. I. Resonances and Disk Gap Sizes. *ApJ* **1994**, *421*, 651. <https://doi.org/10.1086/173679>.
12. Ragusa, E.; Alexander, R.; Calcino, J.; Hirsh, K.; Price, D.J. The evolution of large cavities and disc eccentricity in circumbinary discs. *MNRAS* **2020**, *499*, 3362–3380, [arXiv:astro-ph.EP/2009.10738]. <https://doi.org/10.1093/mnras/staa2954>.
13. Farago, F.; Laskar, J. High-inclination orbits in the secular quadrupolar three-body problem. *MNRAS* **2010**, *401*, 1189–1198, [arXiv:astro-ph.EP/0909.2287]. <https://doi.org/10.1111/j.1365-2966.2009.15711.x>.
14. Aly, H.; Dehnen, W.; Nixon, C.; King, A. Misaligned gas discs around eccentric black hole binaries and implications for the final-parsec problem. *MNRAS* **2015**, *449*, 65–76, [arXiv:astro-ph.HE/1501.04623]. <https://doi.org/10.1093/mnras/stv128>.
15. Martin, R.G.; Lubow, S.H. Polar Alignment of a Protoplanetary Disk around an Eccentric Binary. *ApJ* **2017**, *835*, L28, [arXiv:astro-ph.EP/1702.00545]. <https://doi.org/10.3847/2041-8213/835/2/L28>.
16. Cuello, N.; Giuppone, C.A. Planet formation and stability in polar circumbinary discs. *A&A* **2019**, *628*, A119, [arXiv:astro-ph.EP/1906.10579]. <https://doi.org/10.1051/0004-6361/201833976>.
17. Larwood, J.D.; Nelson, R.P.; Papaloizou, J.C.B.; Terquem, C. The tidally induced warping, precession and truncation of accretion discs in binary systems: three-dimensional simulations. *MNRAS* **1996**, *282*, 597–613, [arXiv:astro-ph/astro-ph/9604013]. <https://doi.org/10.1093/mnras/282.2.597>.
18. GRAVITY Collaboration.; Garcia Lopez, R.; Perraut, K.; Caratti O Garatti, A.; Lazareff, B.; Sanchez-Bermudez, J.; Benisty, M.; Dougados, C.; Labadie, L.; Brandner, W.; et al. The wind and the magnetospheric accretion onto the T Tauri star S Coronae Australis at sub-au resolution. *A&A* **2017**, *608*, A78, [arXiv:astro-ph.SR/1709.01348]. <https://doi.org/10.1051/0004-6361/201731058>.
19. Beuzit, J.L.; Vigan, A.; Mouillet, D.; Dohlen, K.; Gratton, R.; Boccaletti, A.; Sauvage, J.F.; Schmid, H.M.; Langlois, M.; Petit, C.; et al. SPHERE: the exoplanet imager for the Very Large Telescope. *A&A* **2019**, *631*, A155, [arXiv:astro-ph.IM/1902.04080]. <https://doi.org/10.1051/0004-6361/201935251>.
20. Ragusa, E.; Dipierro, G.; Lodato, G.; Laibe, G.; Price, D.J. On the origin of horseshoes in transitional discs. *MNRAS* **2017**, *464*, 1449–1455, [arXiv:astro-ph.EP/1609.08159]. <https://doi.org/10.1093/mnras/stw2456>.
21. Thun, D.; Kley, W.; Picogna, G. Circumbinary discs: Numerical and physical behaviour. *A&A* **2017**, *604*, A102, [arXiv:astro-ph.EP/1704.08130]. <https://doi.org/10.1051/0004-6361/201730666>.
22. Poblete, P.P.; Cuello, N.; Cuadra, J. Dusty clumps in circumbinary discs. *MNRAS* **2019**, *489*, 2204–2215, [arXiv:astro-ph.EP/1908.05784]. <https://doi.org/10.1093/mnras/stz2297>.
23. Hirsh, K.; Price, D.J.; Gonzalez, J.F.; Ubeira-Gabellini, M.G.; Ragusa, E. On the cavity size in circumbinary discs. *MNRAS* **2020**, *498*, 2936–2947, [arXiv:astro-ph.EP/2008.08008]. <https://doi.org/10.1093/mnras/staa2536>.
24. Ragusa, E.; Fasano, D.; Toci, C.; Duchêne, G.; Cuello, N.; Villenave, M.; van der Plas, G.; Lodato, G.; Ménard, F.; Price, D.J.; et al. Circumbinary and circumstellar discs around the eccentric binary IRAS 04158+2805 - a testbed for binary-disc interaction. *MNRAS* **2021**, *507*, 1157–1174, [arXiv:astro-ph.SR/2107.13566]. <https://doi.org/10.1093/mnras/stab2179>.
25. Smallwood, J.L.; Nealon, R.; Chen, C.; Martin, R.G.; Bi, J.; Dong, R.; Pinte, C. GW Ori: circumtriple rings and planets. *MNRAS* **2021**, *508*, 392–407, [arXiv:astro-ph.EP/2109.09776]. <https://doi.org/10.1093/mnras/stab2624>.
26. Ceppi, S.; Longarini, C.; Lodato, G.; Cuello, N.; Lubow, S.H. Precession and polar alignment of accretion discs in triple (or multiple) stellar systems. *MNRAS* **2023**, *520*, 5817–5827, [arXiv:astro-ph.EP/2302.03411]. <https://doi.org/10.1093/mnras/stad444>.
27. Toci, C.; Ceppi, S.; Cuello, N.; Duchêne, G.; Ragusa, E.; Lodato, G.; Farina, F.; Ménard, F.; Aly, H. Orbital dynamics in the GG Tau A system: Investigating its enigmatic disc. *A&A* **2024**, *688*, A102, [arXiv:astro-ph.EP/2404.07565]. <https://doi.org/10.1051/0004-6361/202348470>.
28. Price, D.J.; Cuello, N.; Pinte, C.; Mentiplay, D.; Casassus, S.; Christiaens, V.; Kennedy, G.M.; Cuadra, J.; Sebastian Perez, M.; Marino, S.; et al. Circumbinary, not transitional: on the spiral arms, cavity, shadows, fast radial flows, streamers, and horseshoe in the HD 142527 disc. *MNRAS* **2018**, *477*, 1270–1284, [arXiv:astro-ph.SR/1803.02484]. <https://doi.org/10.1093/mnras/sty647>.
29. Gonzalez, J.F.; van der Plas, G.; Pinte, C.; Cuello, N.; Nealon, R.; Ménard, F.; Revol, A.; Rodet, L.; Langlois, M.; Maire, A.L. Spirals, shadows, and precession in HD 100453 - I. The orbit of the binary. *MNRAS* **2020**, *499*, 3837–3856, [arXiv:astro-ph.EP/2009.10504]. <https://doi.org/10.1093/mnras/staa2938>.
30. Lai, D.; Muñoz, D.J. Circumbinary Accretion: From Binary Stars to Massive Binary Black Holes. *ARA&A* **2023**, *61*, 517–560, [arXiv:astro-ph.HE/2211.00028]. <https://doi.org/10.1146/annurev-astro-052622-022933>.

31. Calcino, J.; Norfolk, B.J.; Price, D.J.; Hilder, T.; Speedie, J.; Pinte, C.; Garg, H.; Teague, R.; Hall, C.; Stadler, J. Observational signatures of circumbinary discs - II. Kinematic signatures in velocity residuals. *MNRAS* **2024**, *534*, 2904–2917, [[arXiv:astro-ph.EP/2407.21309](#)]. <https://doi.org/10.1093/mnras/stae2233>.
32. Penzlin, A.B.T.; Booth, R.A.; Nelson, R.P.; Schäfer, C.M.; Kley, W. Viscous circumbinary protoplanetary discs - I. Structure of the inner cavity. *MNRAS* **2024**, *532*, 3166–3179, [[arXiv:astro-ph.EP/2407.07243](#)]. <https://doi.org/10.1093/mnras/stae1689>.
33. Ragusa, E.; Lynch, E.; Laibe, G.; Longarini, C.; Ceppi, S. Probing the eccentricity in protostellar discs: Modelling kinematics and morphologies. *A&A* **2024**, *686*, A264, [[arXiv:astro-ph.EP/2404.02958](#)]. <https://doi.org/10.1051/0004-6361/202449583>.
34. Duchêne, G.; LeBouquin, J.B.; Ménard, F.; Cuello, N.; Toci, C.; Langlois, M. Full orbital solutions in pre-main sequence high-order multiple systems: GG Tau Ab and UX Tau B. *A&A* **2024**, *686*, A188, [[arXiv:astro-ph.SR/2404.02469](#)]. <https://doi.org/10.1051/0004-6361/202348755>.
35. Birnstiel, T.; Dullemond, C.P.; Brauer, F. Gas- and dust evolution in protoplanetary disks. *A&A* **2010**, *513*, A79, [[arXiv:astro-ph.EP/1002.0335](#)]. <https://doi.org/10.1051/0004-6361/200913731>.
36. Price, D.J. Smoothed particle hydrodynamics and magnetohydrodynamics. *Journal of Computational Physics* **2012**, *231*, 759–794, [[arXiv:astro-ph.IM/1012.1885](#)]. <https://doi.org/10.1016/j.jcp.2010.12.011>.
37. Teyssier, R. Grid-Based Hydrodynamics in Astrophysical Fluid Flows. *ARA&A* **2015**, *53*, 325–364. <https://doi.org/10.1146/annurev-astro-082214-122309>.
38. Lesur, G.; Flock, M.; Ercolano, B.; Lin, M.K.; Yang, C.; Barranco, J.A.; Benítez-Llambay, P.; Goodman, J.; Johansen, A.; Klahr, H.; et al. Hydro-, Magnetohydro-, and Dust-Gas Dynamics of Protoplanetary Disks. In Proceedings of the Protostars and Planets VII; Inutsuka, S.; Aikawa, Y.; Muto, T.; Tomida, K.; Tamura, M., Eds., July 2023, Vol. 534, *Astronomical Society of the Pacific Conference Series*, p. 465, [[arXiv:astro-ph.EP/2203.09821](#)]. <https://doi.org/10.48550/arXiv.2203.09821>.
39. Miotello, A.; Kamp, I.; Birnstiel, T.; Cleeves, L.C.; Kataoka, A. Setting the Stage for Planet Formation: Measurements and Implications of the Fundamental Disk Properties. In Proceedings of the Protostars and Planets VII; Inutsuka, S.; Aikawa, Y.; Muto, T.; Tomida, K.; Tamura, M., Eds., July 2023, Vol. 534, *Astronomical Society of the Pacific Conference Series*, p. 501, [[arXiv:astro-ph.EP/2203.09818](#)]. <https://doi.org/10.48550/arXiv.2203.09818>.
40. Villenave, M.; Ménard, F.; Dent, W.R.F.; Duchêne, G.; Stapelfeldt, K.R.; Benisty, M.; Boehler, Y.; van der Plas, G.; Pinte, C.; Telkamp, Z.; et al. Observations of edge-on protoplanetary disks with ALMA. I. Results from continuum data. *A&A* **2020**, *642*, A164, [[arXiv:astro-ph.SR/2008.06518](#)]. <https://doi.org/10.1051/0004-6361/202038087>.
41. Panque-Carreño, T.; Miotello, A.; van Dishoeck, E.F.; Tabone, B.; Izquierdo, A.F.; Facchini, S. Directly tracing the vertical stratification of molecules in protoplanetary disks. *A&A* **2023**, *669*, A126, [[arXiv:astro-ph.EP/2210.01130](#)]. <https://doi.org/10.1051/0004-6361/202244428>.
42. Pfeil, T.; Birnstiel, T.; Klahr, H. Vertical shear instability with dust evolution and consistent cooling times. On the importance of the initial dust distribution. *A&A* **2024**, *687*, L5, [[arXiv:astro-ph.EP/2406.10335](#)]. <https://doi.org/10.1051/0004-6361/202449323>.
43. Bohlin, R.C.; Savage, B.D.; Drake, J.F. A survey of interstellar H I from Lalpha absorption measurements. II. *ApJ* **1978**, *224*, 132–142. <https://doi.org/10.1086/156357>.
44. Telesco, C.M.; Knacke, R.F. Detection of Silicates in the beta Pictoris Disk. *ApJ* **1991**, *372*, L29. <https://doi.org/10.1086/186016>.
45. Mathis, J.S.; Rumpl, W.; Nordsieck, K.H. The size distribution of interstellar grains. *ApJ* **1977**, *217*, 425–433. <https://doi.org/10.1086/155591>.
46. Epstein, P.S. On the Resistance Experienced by Spheres in their Motion through Gases. *Physical Review* **1924**, *23*, 710–733. <https://doi.org/10.1103/PhysRev.23.710>.
47. Weidenschilling, S.J. Aerodynamics of solid bodies in the solar nebula. *MNRAS* **1977**, *180*, 57–70. <https://doi.org/10.1093/mnras/180.2.57>.
48. Laibe, G.; Gonzalez, J.F.; Maddison, S.T. Revisiting the “radial-drift barrier” of planet formation and its relevance in observed protoplanetary discs. *A&A* **2012**, *537*, A61, [[arXiv:astro-ph.EP/1111.3083](#)]. <https://doi.org/10.1051/0004-6361/201015349>.
49. Benisty, M.; Dominik, C.; Follette, K.; Garufi, A.; Ginski, C.; Hashimoto, J.; Keppler, M.; Kley, W.; Monnier, J. Optical and Near-infrared View of Planet-forming Disks and Protoplanets. In Proceedings of the Protostars and Planets VII; Inutsuka, S.; Aikawa, Y.; Muto, T.; Tomida, K.; Tamura, M., Eds., July 2023, Vol. 534, *Astronomical Society of the Pacific Conference Series*, p. 605, [[arXiv:astro-ph.EP/2203.09991](#)]. <https://doi.org/10.48550/arXiv.2203.09991>.
50. Andrews, S.M. Observations of Protoplanetary Disk Structures. *ARA&A* **2020**, *58*, 483–528, [[arXiv:astro-ph.EP/2001.05007](#)]. <https://doi.org/10.1146/annurev-astro-031220-010302>.
51. Manara, C.F.; Tazzari, M.; Long, F.; Herczeg, G.J.; Lodato, G.; Rota, A.A.; Cazzoletti, P.; van der Plas, G.; Pinilla, P.; Dipierro, G.; et al. Observational constraints on dust disk sizes in tidally truncated protoplanetary disks in multiple systems in the Taurus region. *A&A* **2019**, *628*, A95, [[arXiv:astro-ph.EP/1907.03846](#)]. <https://doi.org/10.1051/0004-6361/201935964>.
52. Akeson, R.L.; Jensen, E.L.N.; Carpenter, J.; Ricci, L.; Laos, E.; Nogueira, N.F.; Suen-Lewis, E.M. Resolved Young Binary Systems and Their Disks. *ApJ* **2019**, *872*, 158, [[arXiv:astro-ph.SR/1901.05029](#)]. <https://doi.org/10.3847/1538-4357/aaff6a>.
53. Zurlo, A.; Cieza, L.A.; Pérez, S.; Christiaens, V.; Williams, J.P.; Guidi, G.; Cánovas, H.; Casassus, S.; Hales, A.; Principe, D.A.; et al. The Ophiuchus DIsco Survey Employing ALMA (ODISEA) - II. The effect of stellar multiplicity on disc properties. *MNRAS* **2020**, *496*, 5089–5100, [[arXiv:astro-ph.SR/2006.16259](#)]. <https://doi.org/10.1093/mnras/staa1886>.
54. Zurlo, A.; Gratton, R.; Pérez, S.; Cieza, L. Observations of planet forming disks in multiple stellar systems. *European Physical Journal Plus* **2023**, *138*, 411, [[arXiv:astro-ph.SR/2304.14450](#)]. <https://doi.org/10.1140/epjp/s13360-023-04041-x>.

55. Rosotti, G.P.; Clarke, C.J. The evolution of photoevaporating viscous discs in binaries. *MNRAS* **2018**, *473*, 5630–5640, [[arXiv:astro-ph.EP/1710.08920](#)]. <https://doi.org/10.1093/mnras/stx2769>.
56. Cuello, N.; Dipierro, G.; Mentiplay, D.; Price, D.J.; Pinte, C.; Cuadra, J.; Laibe, G.; Ménard, F.; Poblete, P.P.; Montesinos, M. Flybys in protoplanetary discs: I. Gas and dust dynamics. *MNRAS* **2019**, *483*, 4114–4139, [[arXiv:astro-ph.EP/1812.00961](#)]. <https://doi.org/10.1093/mnras/sty3325>.
57. Rota, A.A.; Manara, C.F.; Miotello, A.; Lodato, G.; Facchini, S.; Koutoulaki, M.; Herczeg, G.; Long, F.; Tazzari, M.; Cabrit, S.; et al. Observational constraints on gas disc sizes in the protoplanetary discs of multiple systems in the Taurus region. *A&A* **2022**, *662*, A121, [[arXiv:astro-ph.EP/2201.03588](#)]. <https://doi.org/10.1051/0004-6361/202141035>.
58. Zagaria, F.; Rosotti, G.P.; Lodato, G. On dust evolution in planet-forming discs in binary systems - I. Theoretical and numerical modelling: radial drift is faster in binary discs. *MNRAS* **2021**, *504*, 2235–2252, [[arXiv:astro-ph.EP/2104.03022](#)]. <https://doi.org/10.1093/mnras/stab985>.
59. Zagaria, F.; Rosotti, G.P.; Alexander, R.D.; Clarke, C.J. Dust dynamics in planet-forming discs in binary systems. *European Physical Journal Plus* **2023**, *138*, 25, [[arXiv:astro-ph.EP/2212.07711](#)]. <https://doi.org/10.1140/epjp/s13360-022-03616-4>.
60. Cieza, L.A.; Padgett, D.L.; Allen, L.E.; McCabe, C.E.; Brooke, T.Y.; Carey, S.J.; Chapman, N.L.; Fukagawa, M.; Huard, T.L.; Noriga-Crespo, A.; et al. Primordial Circumstellar Disks in Binary Systems: Evidence for Reduced Lifetimes. *ApJ* **2009**, *696*, L84–L88, [[arXiv:astro-ph.SR/0903.3057](#)]. <https://doi.org/10.1088/0004-637X/696/1/L84>.
61. Alexander, R. The Dispersal of Protoplanetary Disks around Binary Stars. *ApJ* **2012**, *757*, L29, [[arXiv:astro-ph.EP/1209.0779](#)]. <https://doi.org/10.1088/2041-8205/757/2/L29>.
62. Ronco, M.P.; Guilera, O.M.; Cuadra, J.; Miller Bertolami, M.M.; Cuello, N.; Fontecilla, C.; Poblete, P.; Bayo, A. Long Live the Disk: Lifetimes of Protoplanetary Disks in Hierarchical Triple-star Systems and a Possible Explanation for HD 98800 B. *ApJ* **2021**, *916*, 113, [[arXiv:astro-ph.EP/2105.09410](#)]. <https://doi.org/10.3847/1538-4357/ac0438>.
63. Cuello, N.; Ménard, F.; Price, D.J. Close encounters: How stellar flybys shape planet-forming discs. *European Physical Journal Plus* **2023**, *138*, 11, [[arXiv:astro-ph.EP/2207.09752](#)]. <https://doi.org/10.1140/epjp/s13360-022-03602-w>.
64. Lindblad, B. On the development of spiral structure in a rotating stellar system. *Stockholms Observatoriums Annaler* **1941**, *13*, 10.1–10.50.
65. Rafikov, R.R. Nonlinear Propagation of Planet-generated Tidal Waves. *ApJ* **2002**, *569*, 997–1008, [[arXiv:astro-ph/astro-ph/0110496](#)]. <https://doi.org/10.1086/339399>.
66. Forgan, D.H.; Ilee, J.D.; Meru, F. Are Elias 2-27’s Spiral Arms Driven by Self-gravity, or by a Companion? A Comparative Spiral Morphology Study. *ApJ* **2018**, *860*, L5, [[arXiv:astro-ph.SR/1805.08041](#)]. <https://doi.org/10.3847/2041-8213/aac7c9>.
67. Muley, D.; Melon Fuksman, J.D.; Klahr, H. Spiral excitation in protoplanetary disks through gap-edge illumination: Three-temperature radiation hydrodynamics and NIR image modeling. *A&A* **2024**, *690*, A355, [[arXiv:astro-ph.EP/2408.16461](#)]. <https://doi.org/10.1051/0004-6361/202451554>.
68. Pinte, C.; Teague, R.; Flaherty, K.; Hall, C.; Facchini, S.; Casassus, S. Kinematic Structures in Planet-Forming Disks. In Proceedings of the Protostars and Planets VII; Inutsuka, S.; Aikawa, Y.; Muto, T.; Tomida, K.; Tamura, M., Eds., July 2023, Vol. 534, *Astronomical Society of the Pacific Conference Series*, p. 645, [[arXiv:astro-ph.EP/2203.09528](#)]. <https://doi.org/10.48550/arXiv.2203.09528>.
69. Kurtovic, N.T.; Pérez, L.M.; Benisty, M.; Zhu, Z.; Zhang, S.; Huang, J.; Andrews, S.M.; Dullemond, C.P.; Isella, A.; Bai, X.N.; et al. The Disk Substructures at High Angular Resolution Project (DSHARP). IV. Characterizing Substructures and Interactions in Disks around Multiple Star Systems. *ApJ* **2018**, *869*, L44, [[arXiv:astro-ph.SR/1812.04536](#)]. <https://doi.org/10.3847/2041-8213/aaf746>.
70. Borchert, E.M.A.; Price, D.J.; Pinte, C.; Cuello, N. Sustained FU Orionis-type outbursts from colliding discs in stellar flybys. *MNRAS* **2022**, *517*, 4436–4446, [[arXiv:astro-ph.SR/2210.01143](#)]. <https://doi.org/10.1093/mnras/stac2872>.
71. Smallwood, J.L.; Nealon, R.; Cuello, N.; Dong, R.; Booth, R.A. Formation of misaligned second-generation discs through fly-by encounters. *MNRAS* **2024**, *527*, 2094–2109, [[arXiv:astro-ph.EP/2310.03327](#)]. <https://doi.org/10.1093/mnras/stad3057>.
72. Ménard, F.; Cuello, N.; Ginski, C.; van der Plas, G.; Villenave, M.; Gonzalez, J.F.; Pinte, C.; Benisty, M.; Boccaletti, A.; Price, D.J.; et al. Ongoing flyby in the young multiple system UX Tauri. *A&A* **2020**, *639*, L1, [[arXiv:astro-ph.SR/2006.02439](#)]. <https://doi.org/10.1051/0004-6361/202038356>.
73. Bate, M.R.; Bonnell, I.A.; Clarke, C.J.; Lubow, S.H.; Ogilvie, G.I.; Pringle, J.E.; Tout, C.A. Observational implications of precessing protostellar discs and jets. *MNRAS* **2000**, *317*, 773–781, [[arXiv:astro-ph/astro-ph/0005333](#)]. <https://doi.org/10.1046/j.1365-8711.2000.03648.x>.
74. Lubow, S.H.; Ogilvie, G.I. On the Tilting of Protostellar Disks by Resonant Tidal Effects. *ApJ* **2000**, *538*, 326–340, [[arXiv:astro-ph/astro-ph/0003028](#)]. <https://doi.org/10.1086/309101>.
75. Papaloizou, J.C.B.; Terquem, C. On the dynamics of tilted discs around young stars. *MNRAS* **1995**, *274*, 987–1001. <https://doi.org/10.1093/mnras/274.4.987>.
76. Martin, R.G.; Nixon, C.; Lubow, S.H.; Armitage, P.J.; Price, D.J.; Doğan, S.; King, A. The Kozai-Lidov Mechanism in Hydrodynamical Disks. *ApJ* **2014**, *792*, L33, [[arXiv:astro-ph.EP/1409.1226](#)]. <https://doi.org/10.1088/2041-8205/792/2/L33>.
77. Facchini, S.; Lodato, G.; Price, D.J. Wave-like warp propagation in circumbinary discs - I. Analytic theory and numerical simulations. *MNRAS* **2013**, *433*, 2142–2156, [[arXiv:astro-ph.SR/1306.4331](#)]. <https://doi.org/10.1093/mnras/stt877>.
78. Czekala, I.; Chiang, E.; Andrews, S.M.; Jensen, E.L.N.; Torres, G.; Wilner, D.J.; Stassun, K.G.; Macintosh, B. The Degree of Alignment between Circumbinary Disks and Their Binary Hosts. *ApJ* **2019**, *883*, 22, [[arXiv:astro-ph.EP/1906.03269](#)]. <https://doi.org/10.3847/1538-4357/ab287b>.

79. Ceppi, S.; Cuello, N.; Lodato, G.; Longarini, C.; Price, D.J.; Elseder, D.; Bate, M.R. Probing initial distributions of orbital eccentricity and disc misalignment via polar discs. *A&A* **2024**, *682*, A104, [[arXiv:astro-ph.EP/2401.03767](#)]. <https://doi.org/10.1051/0004-6361/202348375>.
80. Weber, P.; Pérez, S.; Guidi, G.; Kurtovic, N.T.; Zurlo, A.; Garufi, A.; Pinilla, P.; Mayama, S.; van Holstein, R.G.; Dullemond, C.P.; et al. The SPHERE view of three interacting twin disc systems in polarized light. *MNRAS* **2023**, *518*, 5620–5642, [[arXiv:astro-ph.SR/2211.14322](#)]. <https://doi.org/10.1093/mnras/stac3478>.
81. Ghez, A.M.; McCarthy, D.W.; Patience, J.L.; Beck, T.L. The Multiplicity of Pre-Main-Sequence Stars in Southern Star-forming Regions. *ApJ* **1997**, *481*, 378–385. <https://doi.org/10.1086/304031>.
82. Andrews, S.M.; Huang, J.; Pérez, L.M.; Isella, A.; Dullemond, C.P.; Kurtovic, N.T.; Guzmán, V.V.; Carpenter, J.M.; Wilner, D.J.; Zhang, S.; et al. The Disk Substructures at High Angular Resolution Project (DSHARP). I. Motivation, Sample, Calibration, and Overview. *ApJ* **2018**, *869*, L41, [[arXiv:astro-ph.SR/1812.04040](#)]. <https://doi.org/10.3847/2041-8213/aaf741>.
83. Stapelfeldt, K.; Burrows, C.J.; Krist, J.E.; WFPC2 Science Team. Hubble Space Telescope Imaging of the Disks and Jets of Taurus Young Stellar Objects. In Proceedings of the Herbig-Haro Flows and the Birth of Stars; Reipurth, B.; Bertout, C., Eds., January 1997, Vol. 182, *IAU Symposium*, pp. 355–364.
84. Cazzoletti, P.; Manara, C.F.; Liu, H.B.; van Dishoeck, E.F.; Facchini, S.; Alcalà, J.M.; Ansdel, M.; Testi, L.; Williams, J.P.; Carrasco-González, C.; et al. ALMA survey of Class II protoplanetary disks in Corona Australis: a young region with low disk masses. *A&A* **2019**, *626*, A11, [[arXiv:astro-ph.EP/1904.02409](#)]. <https://doi.org/10.1051/0004-6361/201935273>.
85. Close, L.M.; Dutrey, A.; Roddier, F.; Guilloteau, S.; Roddier, C.; Northcott, M.; Ménard, F.; Duvert, G.; Graves, J.E.; Potter, D. Adaptive Optics Imaging of the Circumbinary Disk around the T Tauri Binary UY Aurigae: Estimates of the Binary Mass and Circumbinary Dust Grain Size Distribution. *ApJ* **1998**, *499*, 883–888. <https://doi.org/10.1086/305672>.
86. Tang, Y.W.; Dutrey, A.; Guilloteau, S.; Piétu, V.; Di Folco, E.; Beck, T.; Ho, P.T.P.; Boehler, Y.; Gueth, F.; Bary, J.; et al. Circumbinary Ring, Circumstellar Disks, and Accretion in the Binary System UY Aurigae. *ApJ* **2014**, *793*, 10, [[arXiv:astro-ph.GA/1407.4561](#)]. <https://doi.org/10.1088/0004-637X/793/1/10>.
87. White, R.J.; Ghez, A.M. Observational Constraints on the Formation and Evolution of Binary Stars. *ApJ* **2001**, *556*, 265–295, [[arXiv:astro-ph/astro-ph/0103098](#)]. <https://doi.org/10.1086/321542>.
88. Chen, X.P.; Henning, T.; van Boekel, R.; Grady, C.A. VLT/NACO adaptive optics imaging of the Herbig Ae star HD 100453. *A&A* **2006**, *445*, 331–335. <https://doi.org/10.1051/0004-6361:20054122>.
89. Wagner, K.; Apai, D.; Kasper, M.; Robberto, M. Discovery of a Two-armed Spiral Structure in the Gapped Disk around Herbig Ae Star HD 100453. *ApJ* **2015**, *813*, L2, [[arXiv:astro-ph.EP/1510.02212](#)]. <https://doi.org/10.1088/2041-8205/813/1/L2>.
90. Jensen, E.L.N.; Koerner, D.W.; Mathieu, R.D. High-Resolution Imaging of Circumstellar Gas and Dust in UZ Tauri: Comparing Binary and Single-Star Disk Properties. *AJ* **1996**, *111*, 2431. <https://doi.org/10.1086/117977>.
91. Leinert, C.; Zinnecker, H.; Weitzel, N.; Christou, J.; Ridgway, S.T.; Jameson, R.; Haas, M.; Lenzen, R. A systematic search for young binaries in Taurus. *A&A* **1993**, *278*, 129–149.
92. Dutrey, A.; Guilloteau, S.; Simon, M. Images of the GG Tauri rotating ring. *A&A* **1994**, *286*, 149–159.
93. Di Folco, E.; Dutrey, A.; Guilloteau, S.; Le Bouquin, J.B.; Lacour, S.; Berger, J.P.; Köhler, R.; Piétu, V. Planet formation in multiple stellar systems: GG Tau A. In Proceedings of the SF2A-2014: Proceedings of the Annual meeting of the French Society of Astronomy and Astrophysics; Ballet, J.; Martins, F.; Bournaud, F.; Monier, R.; Reyé, C., Eds., December 2014, pp. 135–138.
94. Roddier, C.; Roddier, F.; Northcott, M.J.; Graves, J.E.; Jim, K. Adaptive Optics Imaging of GG Tauri: Optical Detection of the Circumbinary Ring. *ApJ* **1996**, *463*, 326. <https://doi.org/10.1086/177245>.
95. Silber, J.; Gledhill, T.; Duchêne, G.; Ménard, F. Near-Infrared Imaging Polarimetry of the GG Tauri Circumbinary Ring. *ApJ* **2000**, *536*, L89–L92, [[arXiv:astro-ph/astro-ph/0005303](#)]. <https://doi.org/10.1086/312731>.
96. Beck, T.L.; Bary, J.S.; Dutrey, A.; Piétu, V.; Guilloteau, S.; Lubow, S.H.; Simon, M. Circumbinary Gas Accretion onto a Central Binary: Infrared Molecular Hydrogen Emission from GG Tau A. *ApJ* **2012**, *754*, 72, [[arXiv:astro-ph.SR/1205.1526](#)]. <https://doi.org/10.1088/0004-637X/754/1/72>.
97. Keppler, M.; Penzlin, A.; Benisty, M.; van Boekel, R.; Henning, T.; van Holstein, R.G.; Kley, W.; Garufi, A.; Ginski, C.; Brandner, W.; et al. Gap, shadows, spirals, and streamers: SPHERE observations of binary-disk interactions in GG Tauri A. *A&A* **2020**, *639*, A62, [[arXiv:astro-ph.SR/2005.09037](#)]. <https://doi.org/10.1051/0004-6361/202038032>.
98. Mathieu, R.D.; Adams, F.C.; Latham, D.W. The T Tauri Spectroscopic Binary GW Orionis. *AJ* **1991**, *101*, 2184. <https://doi.org/10.1086/115841>.
99. Mathieu, R.D.; Adams, F.C.; Fuller, G.A.; Jensen, E.L.N.; Koerner, D.W.; Sargent, A.I. Submillimeter Continuum Observations of the T Tauri Spectroscopic Binary GW Orionis. *AJ* **1995**, *109*, 2655. <https://doi.org/10.1086/117479>.
100. Berger, J.P.; Monnier, J.D.; Millan-Gabet, R.; Renard, S.; Pedretti, E.; Traub, W.; Bechet, C.; Benisty, M.; Carleton, N.; Haguenauer, P.; et al. First astronomical unit scale image of the GW Orionis triple system. Direct detection of a new stellar companion. *A&A* **2011**, *529*, L1, [[arXiv:astro-ph.SR/1103.3888](#)]. <https://doi.org/10.1051/0004-6361/201016219>.
101. Kraus, S.; Kreplin, A.; Young, A.K.; Bate, M.R.; Monnier, J.D.; Harries, T.J.; Avenhaus, H.; Kluska, J.; Laws, A.S.E.; Rich, E.A.; et al. A triple-star system with a misaligned and warped circumstellar disk shaped by disk tearing. *Science* **2020**, *369*, 1233–1238, [[arXiv:astro-ph.SR/2004.01204](#)]. <https://doi.org/10.1126/science.aba4633>.
102. Fukagawa, M.; Tamura, M.; Itoh, Y.; Kudo, T.; Imaeda, Y.; Oasa, Y.; Hayashi, S.S.; Hayashi, M. Near-Infrared Images of Protoplanetary Disk Surrounding HD 142527. *ApJ* **2006**, *636*, L153–L156. <https://doi.org/10.1086/500128>.

103. Biller, B.; Lacour, S.; Juhász, A.; Benisty, M.; Chauvin, G.; Olofsson, J.; Pott, J.U.; Müller, A.; Sicilia-Aguilar, A.; Bonnefoy, M.; et al. A Likely Close-in Low-mass Stellar Companion to the Transitional Disk Star HD 142527. *ApJ* **2012**, *753*, L38, [[arXiv:astro-ph.SR/1206.2654](#)]. <https://doi.org/10.1088/2041-8205/753/2/L38>.
104. Marino, S.; Perez, S.; Casassus, S. Shadows Cast by a Warp in the HD 142527 Protoplanetary Disk. *ApJ* **2015**, *798*, L44, [[arXiv:astro-ph.EP/1412.4632](#)]. <https://doi.org/10.1088/2041-8205/798/2/L44>.
105. Avenhaus, H.; Quanz, S.P.; Schmid, H.M.; Dominik, C.; Stolker, T.; Ginski, C.; de Boer, J.; Szulágyi, J.; Garufi, A.; Zurlo, A.; et al. Exploring Dust around HD 142527 down to 0."025 (4 au) Using SPHERE/ZIMPOL. *AJ* **2017**, *154*, 33, [[arXiv:astro-ph.EP/1705.09680](#)]. <https://doi.org/10.3847/1538-3881/aa7560>.
106. Torres, G.; Stefanik, R.P.; Latham, D.W.; Mazeh, T. Study of Spectroscopic Binaries with TODCOR. IV. The Multiplicity of the Young Nearby Star HD 98800. *ApJ* **1995**, *452*, 870. <https://doi.org/10.1086/176355>.
107. Koerner, D.W.; Jensen, E.L.N.; Cruz, K.L.; Guild, T.B.; Gultekin, K. A Single Circumbinary Disk in the HD 98800 Quadruple System. *ApJ* **2000**, *533*, L37–L40, [[arXiv:astro-ph/astro-ph/0002227](#)]. <https://doi.org/10.1086/312593>.
108. Gaia Collaboration.; Prusti, T.; de Bruijne, J.H.J.; Brown, A.G.A.; Vallenari, A.; Babusiaux, C.; Bailer-Jones, C.A.L.; Bastian, U.; Biermann, M.; Evans, D.W.; et al. The Gaia mission. *A&A* **2016**, *595*, A1, [[arXiv:astro-ph.IM/1609.04153](#)]. <https://doi.org/10.1051/0004-6361/201629272>.
109. Sullivan, K.; Prato, L.; Edwards, S.; Avilez, I.; Schaefer, G.H. S and VV Corona Australis: Spectroscopic Variability in Two Young Binary Star Systems. *ApJ* **2019**, *884*, 28, [[arXiv:astro-ph.SR/1908.06135](#)]. <https://doi.org/10.3847/1538-4357/ab3c52>.
110. Zhang, Y.; Ginski, C.; Huang, J.; Zurlo, A.; Beust, H.; Bae, J.; Benisty, M.; Garufi, A.; Hogerheijde, M.R.; van Holstein, R.G.; et al. Disk Evolution Study Through Imaging of Nearby Young Stars (DESTINYS): Diverse outcomes of binary-disk interactions. *A&A* **2023**, *672*, A145, [[arXiv:astro-ph.SR/2302.12824](#)]. <https://doi.org/10.1051/0004-6361/202245577>.
111. Gupta, A.; Miotello, A.; Manara, C.F.; Williams, J.P.; Facchini, S.; Beccari, G.; Birnstiel, T.; Ginski, C.; Hacar, A.; Küffmeier, M.; et al. Reflections on nebulae around young stars. A systematic search for late-stage infall of material onto Class II disks. *A&A* **2023**, *670*, L8, [[arXiv:astro-ph.SR/2301.02994](#)]. <https://doi.org/10.1051/0004-6361/202245254>.
112. Gupta, A.; Miotello, A.; Williams, J.P.; Birnstiel, T.; Küffmeier, M.; Yen, H.W. TIPSY: Trajectory of Infalling Particles in Streamers around Young stars. Dynamical analysis of the streamers around S CrA and HL Tau. *A&A* **2024**, *683*, A133, [[arXiv:astro-ph.SR/2401.10403](#)]. <https://doi.org/10.1051/0004-6361/202348007>.
113. Hartigan, P.; Kenyon, S.J. A Spectroscopic Survey of Subarcsecond Binaries in the Taurus-Auriga Dark Cloud with the Hubble Space Telescope. *ApJ* **2003**, *583*, 334–357, [[arXiv:astro-ph/astro-ph/0209608](#)]. <https://doi.org/10.1086/345293>.
114. Hioki, T.; Itoh, Y.; Oasa, Y.; Fukagawa, M.; Kudo, T.; Mayama, S.; Funayama, H.; Hayashi, M.; Hayashi, S.S.; Pyo, T.S.; et al. Near-Infrared Coronagraphic Observations of the T Tauri Binary System UY Aur. *AJ* **2007**, *134*, 880–885, [[arXiv:astro-ph/0705.3940](#)]. <https://doi.org/10.1086/519737>.
115. Long, F.; Herczeg, G.J.; Harsono, D.; Pinilla, P.; Tazzari, M.; Manara, C.F.; Pascucci, I.; Cabrit, S.; Nisini, B.; Johnstone, D.; et al. Compact Disks in a High-resolution ALMA Survey of Dust Structures in the Taurus Molecular Cloud. *ApJ* **2019**, *882*, 49, [[arXiv:astro-ph.SR/1906.10809](#)]. <https://doi.org/10.3847/1538-4357/ab2d2d>.
116. Pyo, T.S.; Hayashi, M.; Beck, T.L.; Davis, C.J.; Takami, M. [Fe II] Emissions Associated with the Young Interacting Binary UY Aurigae. *ApJ* **2014**, *786*, 63, [[arXiv:astro-ph.SR/1403.3474](#)]. <https://doi.org/10.1088/0004-637X/786/1/63>.
117. Garufi, A.; Ginski, C.; van Holstein, R.G.; Benisty, M.; Manara, C.F.; Pérez, S.; Pinilla, P.; Ribas, Á.; Weber, P.; Williams, J.; et al. The SPHERE view of the Taurus star-forming region. The full census of planet-forming disks with GTO and DESTINYS programs. *A&A* **2024**, *685*, A53, [[arXiv:astro-ph.GA/2403.02158](#)]. <https://doi.org/10.1051/0004-6361/202347586>.
118. Herczeg, G.J.; Hillenbrand, L.A. An Optical Spectroscopic Study of T Tauri Stars. I. Photospheric Properties. *ApJ* **2014**, *786*, 97, [[arXiv:astro-ph.SR/1403.1675](#)]. <https://doi.org/10.1088/0004-637X/786/2/97>.
119. Schaefer, G.H.; Beck, T.L.; Prato, L.; Simon, M. Orbital Motion, Variability, and Masses in the T Tauri Triple System. *AJ* **2020**, *160*, 35, [[arXiv:astro-ph.SR/2006.03183](#)]. <https://doi.org/10.3847/1538-3881/ab93be>.
120. Yamaguchi, M.; Tsukagoshi, T.; Muto, T.; Nomura, H.; Nakazato, T.; Ikeda, S.; Tamura, M.; Kawabe, R. ALMA Super-resolution Imaging of T Tau: r = 12 au Gap in the Compact Dust Disk around T Tau N. *ApJ* **2021**, *923*, 121, [[arXiv:astro-ph.EP/2110.00974](#)]. <https://doi.org/10.3847/1538-4357/ac2bfd>.
121. Beck, T.L.; Schaefer, G.H.; Guilloteau, S.; Simon, M.; Dutrey, A.; Di Folco, E.; Chapillon, E. On the Nature of the T Tauri Triple System. *ApJ* **2020**, *902*, 132, [[arXiv:astro-ph.SR/2009.03861](#)]. <https://doi.org/10.3847/1538-4357/abb5f5>.
122. Momose, M.; Ohashi, N.; Kawabe, R.; Hayashi, M.; Nakano, T. The Dispersing Cloud Core around T Tauri. *ApJ* **1996**, *470*, 1001. <https://doi.org/10.1086/177925>.
123. Kouwenhoven, M.B.N.; Brown, A.G.A.; Zinnecker, H.; Kaper, L.; Portegies Zwart, S.F. The primordial binary population. I. A near-infrared adaptive optics search for close visual companions to A star members of Scorpius OB2. *A&A* **2005**, *430*, 137–154, [[arXiv:astro-ph/astro-ph/0410106](#)]. <https://doi.org/10.1051/0004-6361:20048124>.
124. Benisty, M.; Stolker, T.; Pohl, A.; de Boer, J.; Lesur, G.; Dominik, C.; Dullemond, C.P.; Langlois, M.; Min, M.; Wagner, K.; et al. Shadows and spirals in the protoplanetary disk HD 100453. *A&A* **2017**, *597*, A42, [[arXiv:astro-ph.EP/1610.10089](#)]. <https://doi.org/10.1051/0004-6361/201629798>.
125. van der Plas, G.; Ménard, F.; Gonzalez, J.F.; Perez, S.; Rodet, L.; Pinte, C.; Cieza, L.; Casassus, S.; Benisty, M. ALMA study of the HD 100453 AB system and the tidal interaction of the companion with the disk. *A&A* **2019**, *624*, A33, [[arXiv:astro-ph.SR/1902.00720](#)]. <https://doi.org/10.1051/0004-6361/201834134>.

126. Rosotti, G.P.; Benisty, M.; Juhász, A.; Teague, R.; Clarke, C.; Dominik, C.; Dullemond, C.P.; Klaassen, P.D.; Matrà, L.; Stolk, T. Spiral arms in the protoplanetary disc HD100453 detected with ALMA: evidence for binary-disc interaction and a vertical temperature gradient. *MNRAS* **2020**, *491*, 1335–1347, [[arXiv:astro-ph.EP/1911.00518](#)]. <https://doi.org/10.1093/mnras/stz3090>.
127. Dong, R.; Zhu, Z.; Fung, J.; Rafikov, R.; Chiang, E.; Wagner, K. An M Dwarf Companion and Its Induced Spiral Arms in the HD 100453 Protoplanetary Disk. *ApJ* **2016**, *816*, L12, [[arXiv:astro-ph.SR/1512.04949](#)]. <https://doi.org/10.3847/2041-8205/816/1/L12>.
128. Min, M.; Stolk, T.; Dominik, C.; Benisty, M. Connecting the shadows: probing inner disk geometries using shadows in transitional disks. *A&A* **2017**, *604*, L10, [[arXiv:astro-ph.EP/1704.01844](#)]. <https://doi.org/10.1051/0004-6361/201730949>.
129. Wagner, K.; Dong, R.; Sheehan, P.; Apai, D.; Kasper, M.; McClure, M.; Morzinski, K.M.; Close, L.; Males, J.; Hinz, P.; et al. The Orbit of the Companion to HD 100453A: Binary-driven Spiral Arms in a Protoplanetary Disk. *ApJ* **2018**, *854*, 130, [[arXiv:astro-ph.SR/1801.03900](#)]. <https://doi.org/10.3847/1538-4357/aaa767>.
130. Nealon, R.; Cuello, N.; Gonzalez, J.F.; van der Plas, G.; Pinte, C.; Alexander, R.; Ménard, F.; Price, D.J. Spirals, shadows & precession in HD 100453 - II. The hidden companion. *MNRAS* **2020**, *499*, 3857–3867, [[arXiv:astro-ph.EP/2009.10505](#)]. <https://doi.org/10.1093/mnras/staa2721>.
131. Calcino, J.; Price, D.J.; Pinte, C.; Garg, H.; Norfolk, B.J.; Christiaens, V.; Li, H.; Teague, R. Observational signatures of circumbinary discs - I. Kinematics. *MNRAS* **2023**, *523*, 5763–5788, [[arXiv:astro-ph.EP/2306.07909](#)]. <https://doi.org/10.1093/mnras/stad1798>.
132. Artynowicz, P.; Lubow, S.H. Mass Flow through Gaps in Circumbinary Disks. *ApJ* **1996**, *467*, L77. <https://doi.org/10.1086/310200>.
133. Duffell, P.C.; D’Orazio, D.; Derdzinski, A.; Haiman, Z.; MacFadyen, A.; Rosen, A.L.; Zrake, J. Circumbinary Disks: Accretion and Torque as a Function of Mass Ratio and Disk Viscosity. *ApJ* **2020**, *901*, 25, [[arXiv:astro-ph.SR/1911.05506](#)]. <https://doi.org/10.3847/1538-4357/abab95>.
134. Ceppi, S.; Cuello, N.; Lodato, G.; Clarke, C.; Toci, C.; Price, D.J. Accretion rates in hierarchical triple systems with discs. *MNRAS* **2022**, *514*, 906–919, [[arXiv:astro-ph.SR/2205.08784](#)]. <https://doi.org/10.1093/mnras/stac1390>.
135. Young, A.K.; Stevenson, S.; Nixon, C.J.; Rice, K. On the conditions for warping and breaking protoplanetary discs. *MNRAS* **2023**, *525*, 2616–2631, [[arXiv:astro-ph.SR/2306.11809](#)]. <https://doi.org/10.1093/mnras/stad2451>.
136. Alaguero, A.; Cuello, N.; Ménard, F.; Ceppi, S.; Ribas, Á.; Nealon, R.; Vioque, M.; Izquierdo, A.; Miley, J.; Macías, E.; et al. V892 Tau: A tidally perturbed circumbinary disc in a triple stellar system. *A&A* **2024**, *687*, A311, [[arXiv:astro-ph.EP/2405.12593](#)]. <https://doi.org/10.1051/0004-6361/202449683>.
137. Franchini, A.; Lubow, S.H.; Martin, R.G. Circumbinary Disk Inner Radius as a Diagnostic for Disk-Binary Misalignment. *ApJ* **2019**, *880*, L18, [[arXiv:astro-ph.EP/1907.05437](#)]. <https://doi.org/10.3847/2041-8213/ab2fd8>.
138. Prato, L.; Simon, M.; Mazeh, T.; Zucker, S.; McLean, I.S. Component Masses of the Young Spectroscopic Binary UZ Tau E. *ApJ* **2002**, *579*, L99–L102, [[arXiv:astro-ph/astro-ph/0210106](#)]. <https://doi.org/10.1086/345317>.
139. Jensen, E.L.N.; Dhital, S.; Stassun, K.G.; Patience, J.; Herbst, W.; Walter, F.M.; Simon, M.; Basri, G. Periodic Accretion from a Circumbinary Disk in the Young Binary UZ Tau E. *AJ* **2007**, *134*, 241–251, [[arXiv:astro-ph/0704.0307](#)]. <https://doi.org/10.1086/518408>.
140. Jennings, J.; Tazzari, M.; Clarke, C.J.; Booth, R.A.; Rosotti, G.P. Superresolution trends in the ALMA Taurus survey: structured inner discs and compact discs. *MNRAS* **2022**, *514*, 6053–6073, [[arXiv:astro-ph.EP/2206.11308](#)]. <https://doi.org/10.1093/mnras/stac1770>.
141. Phuong, N.T.; Dutrey, A.; Di Folco, E.; Guilloteau, S.; Pierens, A.; Bary, J.; Beck, T.L.; Chapillon, E.; Denis-Alpizar, O.; Diep, P.N.; et al. Planet-induced spirals in the circumbinary disk of GG Tauri A. *A&A* **2020**, *635*, L9. <https://doi.org/10.1051/0004-6361/202037682>.
142. Guilloteau, S.; Dutrey, A.; Simon, M. GG Tauri: the ring world. *A&A* **1999**, *348*, 570–578.
143. Duchêne, G.; McCabe, C.; Ghez, A.M.; Macintosh, B.A. A Multiwavelength Scattered Light Analysis of the Dust Grain Population in the GG Tauri Circumbinary Ring. *ApJ* **2004**, *606*, 969–982, [[arXiv:astro-ph/astro-ph/0401560](#)]. <https://doi.org/10.1086/383126>.
144. Czekala, I.; Andrews, S.M.; Torres, G.; Rodriguez, J.E.; Jensen, E.L.N.; Stassun, K.G.; Latham, D.W.; Wilner, D.J.; Gully-Santiago, M.A.; Grankin, K.N.; et al. The Architecture of the GW Ori Young Triple-star System and Its Disk: Dynamical Masses, Mutual Inclinations, and Recurrent Eclipses. *ApJ* **2017**, *851*, 132, [[arXiv:astro-ph.EP/1710.03153](#)]. <https://doi.org/10.3847/1538-4357/aa9be7>.
145. Prato, L.; Ruiz-Rodríguez, D.; Wasserman, L.H. Orbital Solution for the Spectroscopic Binary in the GW Ori Hierarchical Triple. *ApJ* **2018**, *852*, 38, [[arXiv:astro-ph.SR/1711.09449](#)]. <https://doi.org/10.3847/1538-4357/aa98df>.
146. Bi, J.; van der Marel, N.; Dong, R.; Muto, T.; Martin, R.G.; Smallwood, J.L.; Hashimoto, J.; Liu, H.B.; Nomura, H.; Hasegawa, Y.; et al. GW Ori: Interactions between a Triple-star System and Its Circumtriple Disk in Action. *ApJ* **2020**, *895*, L18, [[arXiv:astro-ph.SR/2004.03135](#)]. <https://doi.org/10.3847/2041-8213/ab8eb4>.
147. Rabago, I.; Zhu, Z.; Lubow, S.; Martin, R.G. Warps and breaks in circumbinary discs. *MNRAS* **2024**, *533*, 360–373, [[arXiv:astro-ph.EP/2310.00459](#)]. <https://doi.org/10.1093/mnras/stae1787>.
148. Casassus, S.; Wright, C.M.; Marino, S.; Maddison, S.T.; Wootten, A.; Roman, P.; Pérez, S.; Pinilla, P.; Wyatt, M.; Moral, V.; et al. A Compact Concentration of Large Grains in the HD 142527 Protoplanetary Dust Trap. *ApJ* **2015**, *812*, 126, [[arXiv:astro-ph.SR/1505.07743](#)]. <https://doi.org/10.1088/0004-637X/812/2/126>.
149. Christiaens, V.; Casassus, S.; Perez, S.; van der Plas, G.; Ménard, F. Spiral Arms in the Disk of HD 142527 from CO Emission Lines with ALMA. *ApJ* **2014**, *785*, L12, [[arXiv:astro-ph.EP/1403.1463](#)]. <https://doi.org/10.1088/2041-8205/785/1/L12>.

150. Casassus, S.; Hales, A.; de Gregorio, I.; Dent, B.; Belloche, A.; Güsten, R.; Ménard, F.; Hughes, A.M.; Wilner, D.; Salinas, V. CO(6-5) and [C i](2-1) pointed observations of five protoplanetary disks: Warm gas in HD 142527. *A&A* **2013**, *553*, A64. <https://doi.org/10.1051/0004-6361/201219644>.
151. Nowak, M.; Rowther, S.; Lacour, S.; Meru, F.; Nealon, R.; Price, D.J. The orbit of HD 142527 B is too compact to explain many of the disc features. *A&A* **2024**, *683*, A6, [[arXiv:astro-ph.SR/2402.03595](#)]. <https://doi.org/10.1051/0004-6361/202347748>.
152. Soderblom, D.R.; Henry, T.J.; Shetrone, M.D.; Jones, B.F.; Saar, S.H. The Age-related Properties of the HD 98800 System. *ApJ* **1996**, *460*, 984. <https://doi.org/10.1086/177026>.
153. Prato, L.; Ghez, A.M.; Piña, R.K.; Telesco, C.M.; Fisher, R.S.; Wizinowich, P.; Lai, O.; Acton, D.S.; Stomski, P. Keck Diffraction-limited Imaging of the Young Quadruple Star System HD 98800. *ApJ* **2001**, *549*, 590–598, [[arXiv:astro-ph/astro-ph/0011135](#)]. <https://doi.org/10.1086/319061>.
154. Torres, C.A.O.; Quast, G.R.; Melo, C.H.F.; Sterzik, M.F. Young Nearby Loose Associations. In *Handbook of Star Forming Regions, Volume II*; Reipurth, B., Ed.; 2008; Vol. 5, p. 757. <https://doi.org/10.48550/arXiv.0808.3362>.
155. Zúñiga-Fernández, S.; Olofsson, J.; Bayo, A.; Haubois, X.; Corral-Santana, J.M.; Lopera-Mejía, A.; Ronco, M.P.; Tokovinin, A.; Gallenne, A.; Kennedy, G.M.; et al. The HD 98800 quadruple pre-main sequence system. Towards full orbital characterisation using long-baseline infrared interferometry. *A&A* **2021**, *655*, A15, [[arXiv:astro-ph.SR/2109.02841](#)]. <https://doi.org/10.1051/0004-6361/202141985>.
156. Akeson, R.L.; Rice, W.K.M.; Boden, A.F.; Sargent, A.I.; Carpenter, J.M.; Bryden, G. The Circumbinary Disk of HD 98800B: Evidence for Disk Warping. *ApJ* **2007**, *670*, 1240–1246, [[arXiv:astro-ph/0708.2390](#)]. <https://doi.org/10.1086/522579>.
157. Andrews, S.M.; Czekala, I.; Wilner, D.J.; Espaillat, C.; Dullemond, C.P.; Hughes, A.M. Truncated Disks in TW Hya Association Multiple Star Systems. *ApJ* **2010**, *710*, 462–469, [[arXiv:astro-ph.SR/0912.3537](#)]. <https://doi.org/10.1088/0004-637X/710/1/462>.
158. Ribas, Á.; Macías, E.; Espaillat, C.C.; Duchêne, G. Long-lived Protoplanetary Disks in Multiple Systems: The VLA View of HD 98800. *ApJ* **2018**, *865*, 77, [[arXiv:astro-ph.SR/1808.02493](#)]. <https://doi.org/10.3847/1538-4357/aad81b>.
159. Kennedy, G.M.; Matrà, L.; Facchini, S.; Milli, J.; Panić, O.; Price, D.; Wilner, D.J.; Wyatt, M.C.; Yelverton, B.M. A circumbinary protoplanetary disk in a polar configuration. *Nature Astronomy* **2019**, *3*, 230–235. <https://doi.org/10.1038/s41550-018-0667-x>.
160. Smallwood, J.L.; Lin, M.K.; Aly, H.; Nealon, R.; Longarini, C. Polar alignment of a dusty circumbinary disc - I. Dust ring formation. *MNRAS* **2024**, *532*, 1068–1086, [[arXiv:astro-ph.EP/2406.06971](#)]. <https://doi.org/10.1093/mnras/stae1462>.
161. Smallwood, J.L.; Nealon, R.; Yen, H.W.; Pinte, C.; Longarini, C.; Aly, H.; Lin, M.K. Observational Signatures of Dust Traffic Jams in Polar-Aligning Circumbinary Disks. *arXiv e-prints* **2024**, p. arXiv:2411.12614, [[arXiv:astro-ph.EP/2411.12614](#)]. <https://doi.org/10.48550/arXiv.2411.12614>.
162. Poblete, P.P.; Calcino, J.; Cuello, N.; Macías, E.; Ribas, Á.; Price, D.J.; Cuadra, J.; Pinte, C. Binary-induced spiral arms inside the disc cavity of AB Aurigae. *MNRAS* **2020**, *496*, 2362–2371, [[arXiv:astro-ph.EP/2005.10722](#)]. <https://doi.org/10.1093/mnras/staa1655>.
163. Dunhill, A.C.; Cuadra, J.; Dougados, C. Precession and accretion in circumbinary discs: the case of HD 104237. *MNRAS* **2015**, *448*, 3545–3554, [[arXiv:astro-ph.SR/1411.0687](#)]. <https://doi.org/10.1093/mnras/stv284>.
164. Gonzalez, J.F.; Laibe, G.; Maddison, S.T. Self-induced dust traps: overcoming planet formation barriers. *MNRAS* **2017**, *467*, 1984–1996, [[arXiv:astro-ph.EP/1701.01115](#)]. <https://doi.org/10.1093/mnras/stx016>.
165. Chachan, Y.; Booth, R.A.; Triaud, A.H.M.J.; Clarke, C. Dust accretion in binary systems: implications for planets and transition discs. *MNRAS* **2019**, *489*, 3896–3904, [[arXiv:astro-ph.EP/1908.11377](#)]. <https://doi.org/10.1093/mnras/stz2404>.
166. Coleman, G.A.L.; Nelson, R.P.; Triaud, A.H.M.J. Dusty circumbinary discs: inner cavity structures and stopping locations of migrating planets. *MNRAS* **2022**, *513*, 2563–2580, [[arXiv:astro-ph.EP/2204.04152](#)]. <https://doi.org/10.1093/mnras/stac1029>.
167. Aly, H.; Lodato, G. Efficient dust ring formation in misaligned circumbinary discs. *MNRAS* **2020**, *492*, 3306–3315, [[arXiv:astro-ph.EP/2001.03066](#)]. <https://doi.org/10.1093/mnras/stz3633>.
168. Aly, H.; Gonzalez, J.F.; Nealon, R.; Longarini, C.; Lodato, G.; Price, D.J. Dust traffic jams in inclined circumbinary protoplanetary discs - I. Morphology and formation theory. *MNRAS* **2021**, *508*, 2743–2757, [[arXiv:astro-ph.EP/2109.13256](#)]. <https://doi.org/10.1093/mnras/stab2794>.
169. Longarini, C.; Lodato, G.; Toci, C.; Aly, H. Dynamical dust traps in misaligned circumbinary discs: analytical theory and numerical simulations. *MNRAS* **2021**, *503*, 4930–4941, [[arXiv:astro-ph.EP/2103.12084](#)]. <https://doi.org/10.1093/mnras/stab843>.
170. Aly, H.; Nealon, R.; Gonzalez, J.F. WIIndI: a Warp-Induced Dust Instability in protoplanetary discs. *MNRAS* **2024**, *527*, 4777–4789, [[arXiv:astro-ph.EP/2311.06182](#)]. <https://doi.org/10.1093/mnras/stad3494>.
171. Dominik, C.; Dullemond, C.P. The bouncing barrier revisited: Impact on key planet formation processes and observational signatures. *A&A* **2024**, *682*, A144, [[arXiv:astro-ph.EP/2312.06000](#)]. <https://doi.org/10.1051/0004-6361/202347716>.
172. Ribas, Á.; Espaillat, C.C.; Macías, E.; Sarro, L.M. Modeling protoplanetary disk SEDs with artificial neural networks. Revisiting the viscous disk model and updated disk masses. *A&A* **2020**, *642*, A171, [[arXiv:astro-ph.SR/2009.03323](#)]. <https://doi.org/10.1051/0004-6361/202038352>.
173. Ginski, C.; Tazaki, R.; Dominik, C.; Stolker, T. Observed Polarized Scattered Light Phase Functions of Planet-forming Disks. *ApJ* **2023**, *953*, 92, [[arXiv:astro-ph.EP/2301.04617](#)]. <https://doi.org/10.3847/1538-4357/acdc97>.
174. Macías, E.; Guerra-Alvarado, O.; Carrasco-González, C.; Ribas, Á.; Espaillat, C.C.; Huang, J.; Andrews, S.M. Characterizing the dust content of disk substructures in TW Hydreae. *A&A* **2021**, *648*, A33, [[arXiv:astro-ph.EP/2102.04648](#)]. <https://doi.org/10.1051/0004-6361/202039812>.

175. Guidi, G.; Isella, A.; Testi, L.; Chandler, C.J.; Liu, H.B.; Schmid, H.M.; Rosotti, G.; Meng, C.; Jennings, J.; Williams, J.P.; et al. Distribution of solids in the rings of the HD 163296 disk: a multiwavelength study. *A&A* **2022**, *664*, A137, [[arXiv:astro-ph.EP/2207.01496](#)]. <https://doi.org/10.1051/0004-6361/202142303>.
176. Jiang, H.; Macías, E.; Guerra-Alvarado, O.M.; Carrasco-González, C. Grain-size measurements in protoplanetary disks indicate fragile pebbles and low turbulence. *A&A* **2024**, *682*, A32, [[arXiv:astro-ph.EP/2311.07775](#)]. <https://doi.org/10.1051/0004-6361/202348271>.
177. Sierra, A.; Pérez, L.M.; Sotomayor, B.; Benisty, M.; Chandler, C.J.; Andrews, S.; Carpenter, J.; Henning, T.; Testi, L.; Ricci, L.; et al. Constraints on the Physical Origin of Large Cavities in Transition Disks from Multiwavelength Dust Continuum Emission. *ApJ* **2024**, *974*, 306, [[arXiv:astro-ph.EP/2408.15407](#)]. <https://doi.org/10.3847/1538-4357/ad7460>.
178. Rivièrre-Marichalar, P.; Fuente, A.; Navarro-Almaida, D.; Baruteau, C. AB Aur: A Rosetta stone for planet formation theories. System chemistry. In Proceedings of the Highlights on Spanish Astrophysics XI; Manteiga, M.; Bellot, L.; Benavidez, P.; de Lorenzo-Cáceres, A.; Fuente, M.A.; Martínez, M.J.; Vázquez Acosta, M.; Dafonte, C., Eds., May 2023, p. 405.
179. Birnstiel, T.; Ormel, C.W.; Dullemond, C.P. Dust size distributions in coagulation/fragmentation equilibrium: numerical solutions and analytical fits. *A&A* **2011**, *525*, A11, [[arXiv:astro-ph.EP/1009.3011](#)]. <https://doi.org/10.1051/0004-6361/201015228>.
180. Ribas, Á.; Clarke, C.J.; Zagaria, F. Inner walls or vortices? Crescent-shaped asymmetries in ALMA observations of protoplanetary discs. *MNRAS* **2024**, *532*, 1752–1764, [[arXiv:astro-ph.EP/2406.14626](#)]. <https://doi.org/10.1093/mnras/stae1534>.
181. Stammler, S.M.; Birnstiel, T. DustPy: A Python Package for Dust Evolution in Protoplanetary Disks. *ApJ* **2022**, *935*, 35, [[arXiv:astro-ph.EP/2207.00322](#)]. <https://doi.org/10.3847/1538-4357/ac7d58>.
182. Vericel, A.; Gonzalez, J.F.; Price, D.J.; Laibe, G.; Pinte, C. Dust growth, fragmentation, and self-induced dust traps in PHANTOM. *MNRAS* **2021**, *507*, 2318–2338, [[arXiv:astro-ph.EP/2108.00878](#)]. <https://doi.org/10.1093/mnras/stab2263>.
183. Michoulier, S.; Gonzalez, J.F.; Price, D.J. Compaction during fragmentation and bouncing produces realistic dust grain porosities in protoplanetary discs. *A&A* **2024**, *688*, A31, [[arXiv:astro-ph.EP/2406.15622](#)]. <https://doi.org/10.1051/0004-6361/202449719>.
184. Clanton, C. Ice Lines in Circumbinary Protoplanetary Disks. *ApJ* **2013**, *768*, L15, [[arXiv:astro-ph.EP/1303.2655](#)]. <https://doi.org/10.1088/2041-8205/768/1/L15>.
185. Pierens, A.; Nelson, R.P. Thermal structure of circumbinary discs: Circumbinary planets should be icy, not rocky. *A&A* **2024**, *686*, A103, [[arXiv:astro-ph.EP/2403.04535](#)]. <https://doi.org/10.1051/0004-6361/202449237>.
186. Gianuzzi, E.; Giuppone, C.; Cuello, N. Circumbinary planets: migration, trapping in mean-motion resonances, and ejection. *A&A* **2023**, *669*, A123, [[arXiv:astro-ph.EP/2211.08520](#)]. <https://doi.org/10.1051/0004-6361/202244902>.
187. Cuello, N.; Sucerquia, M. Alpha Centauri: Disc Dynamics, Planet Stability, Detectability. *Universe* **2024**, *10*, 64, [[arXiv:astro-ph.EP/2401.16003](#)]. <https://doi.org/10.3390/universe10020064>.
188. Doolin, S.; Blundell, K.M. The dynamics and stability of circumbinary orbits. *MNRAS* **2011**, *418*, 2656–2668, [[arXiv:astro-ph.SR/1108.4144](#)]. <https://doi.org/10.1111/j.1365-2966.2011.19657.x>.
189. Chen, C.; Lubow, S.H.; Martin, R.G.; Nixon, C.J. Orbital stability of two circumbinary planets around misaligned eccentric binaries. *MNRAS* **2023**, *521*, 5033–5045, [[arXiv:astro-ph.EP/2303.05379](#)]. <https://doi.org/10.1093/mnras/stad739>.
190. Standing, M.R.; Sairam, L.; Martin, D.V.; Triaud, A.H.M.J.; Correia, A.C.M.; Coleman, G.A.L.; Baycroft, T.A.; Kunovac, V.; Boisse, I.; Cameron, A.C.; et al. Radial-velocity discovery of a second planet in the TOI-1338/BEBOP-1 circumbinary system. *Nature Astronomy* **2023**, *7*, 702–714, [[arXiv:astro-ph.EP/2301.10794](#)]. <https://doi.org/10.1038/s41550-023-01948-4>.
191. Perryman, M.; Hartman, J.; Bakos, G.Á.; Lindegren, L. Astrometric Exoplanet Detection with Gaia. *ApJ* **2014**, *797*, 14, [[arXiv:astro-ph.EP/1411.1173](#)]. <https://doi.org/10.1088/0004-637X/797/1/14>.
192. Gaia Collaboration.; Arenou, F.; Babusiaux, C.; Barstow, M.A.; Faigler, S.; Jorissen, A.; Kervella, P.; Mazeh, T.; Mowlavi, N.; Panuzzo, P.; et al. Gaia Data Release 3. Stellar multiplicity, a teaser for the hidden treasure. *A&A* **2023**, *674*, A34, [[arXiv:astro-ph.SR/2206.05595](#)]. <https://doi.org/10.1051/0004-6361/202243782>.
193. Martin, D.V.; Triaud, A.H.M.J.; Udry, S.; Marmier, M.; Maxted, P.F.L.; Collier Cameron, A.; Hellier, C.; Pepe, F.; Pollacco, D.; Ségransan, D.; et al. The BEBOP radial-velocity survey for circumbinary planets. I. Eight years of CORALIE observations of 47 single-line eclipsing binaries and abundance constraints on the masses of circumbinary planets. *A&A* **2019**, *624*, A68, [[arXiv:astro-ph.EP/1901.01627](#)]. <https://doi.org/10.1051/0004-6361/201833669>.
194. Marzari, F.; Thebault, P. Planets in Binaries: Formation and Dynamical Evolution. *Galaxies* **2019**, *7*, 84, [[arXiv:astro-ph.EP/2002.12006](#)]. <https://doi.org/10.3390/galaxies7040084>.
195. Bonavita, M.; Desidera, S. Frequency of Planets in Binaries. *Galaxies* **2020**, *8*, 16, [[arXiv:astro-ph.EP/2002.11734](#)]. <https://doi.org/10.3390/galaxies8010016>.
196. Moe, M.; Kratter, K.M. Impact of binary stars on planet statistics - I. Planet occurrence rates and trends with stellar mass. *MNRAS* **2021**, *507*, 3593–3611, [[arXiv:astro-ph.EP/1912.01699](#)]. <https://doi.org/10.1093/mnras/stab2328>.
197. Murray, C.D.; Dermott, S.F. *Solar System Dynamics*; 1999. <https://doi.org/10.1017/CBO9781139174817>.
198. Kennedy, G.M.; Wyatt, M.C.; Sibthorpe, B.; Duchêne, G.; Kalas, P.; Matthews, B.C.; Greaves, J.S.; Su, K.Y.L.; Fitzgerald, M.P. 99 Herculis: host to a circumbinary polar-ring debris disc. *MNRAS* **2012**, *421*, 2264–2276, [[arXiv:astro-ph.EP/1201.1911](#)]. <https://doi.org/10.1111/j.1365-2966.2012.20448.x>.
199. Alencar, S.H.P.; Melo, C.H.F.; Dullemond, C.P.; Andersen, J.; Batalha, C.; Vaz, L.P.R.; Mathieu, R.D. The pre-main sequence spectroscopic binary AK Scorpii revisited. *A&A* **2003**, *409*, 1037–1053. <https://doi.org/10.1051/0004-6361:20031229>.

200. Ghez, A.M.; Neugebauer, G.; Matthews, K. The Multiplicity of T Tauri Stars in the Star Forming Regions Taurus-Auriga and Ophiuchus-Scorpius: A 2.2 Micron Speckle Imaging Survey. *AJ* **1993**, *106*, 2005. <https://doi.org/10.1086/116782>.
201. Eisner, J.A.; Hillenbrand, L.A.; Carpenter, J.M.; Wolf, S. Constraining the Evolutionary Stage of Class I Protostars: Multiwave-length Observations and Modeling. *ApJ* **2005**, *635*, 396–421, [arXiv:astro-ph/astro-ph/0508380]. <https://doi.org/10.1086/497161>.
202. Andrews, S.M.; Williams, J.P. A Submillimeter View of Circumstellar Dust Disks in  $\rho$  Ophiuchi. *ApJ* **2007**, *671*, 1800–1812, [arXiv:astro-ph/0708.4185]. <https://doi.org/10.1086/522885>.
203. Stapper, L.M.; Hogerheijde, M.R.; van Dishoeck, E.F.; Mentel, R. The mass and size of Herbig disks as seen by ALMA. *A&A* **2022**, *658*, A112, [arXiv:astro-ph.EP/2112.03297]. <https://doi.org/10.1051/0004-6361/202142164>.
204. Thomas, S.J.; Rodgers, B.; van der Blieck, N.S.; Doppmann, G.; Bouvier, J.; Salvo, C.A.; Beuzit, J.L.; Rigaut, F. A Survey of Herbig Ae/Be Multiplicity. *AJ* **2023**, *165*, 135. <https://doi.org/10.3847/1538-3881/aca803>.
205. Alves, F.O.; Caselli, P.; Girart, J.M.; Segura-Cox, D.; Franco, G.A.P.; Schmiedeke, A.; Zhao, B. Gas flow and accretion via spiral streamers and circumstellar disks in a young binary protostar. *Science* **2019**, *366*, 90–93, [arXiv:astro-ph.SR/1910.01141]. <https://doi.org/10.1126/science.aaw3491>.
206. Zhu, W.; Bernhard, K.; Dai, F.; Fang, M.; Zanazzi, J.J.; Zang, W.; Dong, S.; Hambach, F.J.; Gan, T.; Wu, Z.; et al. Two Candidate KH 15D-like Systems from the Zwicky Transient Facility. *ApJ* **2022**, *933*, L21, [arXiv:astro-ph.SR/2206.00813]. <https://doi.org/10.3847/2041-8213/ac7b2d>.
207. Hu, Z.; Zhu, W.; Dai, F.; Chen, P.; Huang, Y.; Fang, M.; Post, R.S. An Eccentric Binary with a Misaligned Circumbinary Disk. *arXiv e-prints* **2024**, p. arXiv:2409.18296, [arXiv:astro-ph.SR/2409.18296]. <https://doi.org/10.48550/arXiv.2409.18296>.
208. Metchev, S.A.; Hillenbrand, L.A. The Palomar/Keck Adaptive Optics Survey of Young Solar Analogs: Evidence for a Universal Companion Mass Function. *ApJS* **2009**, *181*, 62–109, [arXiv:astro-ph/0808.2982]. <https://doi.org/10.1088/0067-0049/181/1/62>.
209. Kraus, S.; Calvet, N.; Hartmann, L.; Hofmann, K.H.; Kreplin, A.; Monnier, J.D.; Weigelt, G. On the Nature of the Herbig B[e] Star Binary System V921 Scorpii: Discovery of a Close Companion and Relation to the Large-scale Bipolar Nebula. *ApJ* **2012**, *746*, L2, [arXiv:astro-ph.SR/1201.2420]. <https://doi.org/10.1088/2041-8205/746/1/L2>.
210. Barenfeld, S.A.; Carpenter, J.M.; Ricci, L.; Isella, A. ALMA Observations of Circumstellar Disks in the Upper Scorpius OB Association. *ApJ* **2016**, *827*, 142, [arXiv:astro-ph.EP/1605.05772]. <https://doi.org/10.3847/0004-637X/827/2/142>.
211. Davies, C.L. Star-disc (mis-)alignment in Rho Oph and Upper Sco: insights from spatially resolved disc systems with K2 rotation periods. *MNRAS* **2019**, *484*, 1926–1935, [arXiv:astro-ph.SR/1901.01929]. <https://doi.org/10.1093/mnras/stz086>.
212. Daemgen, S.; Petr-Gotzens, M.G.; Correia, S.; Teixeira, P.S.; Brandner, W.; Kley, W.; Zinnecker, H. Protoplanetary disk evolution and stellar parameters of T Tauri binaries in Chamaeleon I. *A&A* **2013**, *554*, A43, [arXiv:astro-ph.SR/1304.1150]. <https://doi.org/10.1051/0004-6361/201321220>.
213. Kraus, A.L.; Hillenbrand, L.A. The Role of Mass and Environment in Multiple-Star Formation: A 2MASS Survey of Wide Multiplicity in Three Young Associations. *ApJ* **2007**, *662*, 413–430, [arXiv:astro-ph/astro-ph/0702545]. <https://doi.org/10.1086/516835>.
214. Akeson, R.L.; Jensen, E.L.N. Circumstellar Disks around Binary Stars in Taurus. *ApJ* **2014**, *784*, 62, [arXiv:astro-ph.SR/1402.5363]. <https://doi.org/10.1088/0004-637X/784/1/62>.
215. Wheelwright, H.E.; Vink, J.S.; Oudmaijer, R.D.; Drew, J.E. On the alignment between the circumstellar disks and orbital planes of Herbig Ae/Be binary systems. *A&A* **2011**, *532*, A28, [arXiv:astro-ph.SR/1106.3949]. <https://doi.org/10.1051/0004-6361/201116996>.
216. Guenther, E.W.; Esposito, M.; Mundt, R.; Covino, E.; Alcalá, J.M.; Cusano, F.; Stecklum, B. Pre-main sequence spectroscopic binaries suitable for VLTI observations. *A&A* **2007**, *467*, 1147–1155, [arXiv:astro-ph/astro-ph/0702268]. <https://doi.org/10.1051/0004-6361:20065686>.
217. Dunham, M.M.; Offner, S.S.R.; Pineda, J.E.; Bourke, T.L.; Tobin, J.J.; Arce, H.G.; Chen, X.; Di Francesco, J.; Johnstone, D.; Lee, K.I.; et al. An ALMA Search for Substructure, Fragmentation, and Hidden Protostars in Starless Cores in Chamaeleon I. *ApJ* **2016**, *823*, 160, [arXiv:astro-ph.GA/1604.04027]. <https://doi.org/10.3847/0004-637X/823/2/160>.
218. D’Alessio, P.; Hartmann, L.; Calvet, N.; Franco-Hernández, R.; Forrest, W.J.; Sargent, B.; Furlan, E.; Uchida, K.; Green, J.D.; Watson, D.M.; et al. The Truncated Disk of CoKu Tau/4. *ApJ* **2005**, *621*, 461–472, [arXiv:astro-ph/astro-ph/0411522]. <https://doi.org/10.1086/427490>.
219. Ireland, M.J.; Kraus, A.L. The Disk Around CoKu Tauri/4: Circumbinary, Not Transitional. *ApJ* **2008**, *678*, L59, [arXiv:astro-ph/0803.2044]. <https://doi.org/10.1086/588216>.
220. Gillen, E.; Aigrain, S.; McQuillan, A.; Bouvier, J.; Hodgkin, S.; Alencar, S.H.P.; Terquem, C.; Southworth, J.; Gibson, N.P.; Cody, A.; et al. CoRoT 223992193: A new, low-mass, pre-main sequence eclipsing binary with evidence of a circumbinary disk. *A&A* **2014**, *562*, A50, [arXiv:astro-ph.SR/1311.3990]. <https://doi.org/10.1051/0004-6361/201322493>.
221. Bouvier, J.; Tessier, E.; Cabrit, S. Sub-arcsecond images of the young star DD Tauri at optical and near-IR wavelengths. *A&A* **1992**, *261*, 451–456.
222. Kutra, T.; Prato, L.; Tofflemire, B.M.; Akeson, R.; Schaefer, G.H.; Tang, S.Y.; Segura-Cox, D.; Johns-Krull, C.M.; Kraus, A.; Andrews, S.; et al. Sites of Planet Formation in Binary Systems. II. Double the Disks in DF Tau. *arXiv e-prints* **2024**, p. arXiv:2411.05203, [arXiv:astro-ph.SR/2411.05203]. <https://doi.org/10.48550/arXiv.2411.05203>.

223. Pascucci, I.; Testi, L.; Herczeg, G.J.; Long, F.; Manara, C.F.; Helder, N.; Mulders, G.D.; Krijt, S.; Ciesla, F.; Henning, T.; et al. A Steeper than Linear Disk Mass-Stellar Mass Scaling Relation. *ApJ* **2016**, *831*, 125, [[arXiv:astro-ph.EP/1608.03621](#)]. <https://doi.org/10.3847/0004-637X/831/2/125>.
224. Mathieu, R.D.; Stassun, K.; Basri, G.; Jensen, E.L.N.; Johns-Krull, C.M.; Valenti, J.A.; Hartmann, L.W. The Classical T Tauri Spectroscopic Binary DQ Tau.I.Orbital Elements and Light Curves. *AJ* **1997**, *113*, 1841. <https://doi.org/10.1086/118395>.
225. Guilloteau, S.; Dutrey, A.; Piétu, V.; Boehler, Y. A dual-frequency sub-arcsecond study of proto-planetary disks at mm wavelengths: first evidence for radial variations of the dust properties. *A&A* **2011**, *529*, A105, [[arXiv:astro-ph.GA/1103.1296](#)]. <https://doi.org/10.1051/0004-6361/201015209>.
226. Ratzka, T.; Köhler, R.; Leinert, C. A multiplicity survey of the  $\rho$  Ophiuchi molecular clouds. *A&A* **2005**, *437*, 611–626, [[arXiv:astro-ph/astro-ph/0504593](#)]. <https://doi.org/10.1051/0004-6361:20042107>.
227. Cox, E.G.; Harris, R.J.; Looney, L.W.; Chiang, H.F.; Chandler, C.; Kratter, K.; Li, Z.Y.; Perez, L.; Tobin, J.J. Protoplanetary Disks in  $\rho$  Ophiuchus as Seen from ALMA. *ApJ* **2017**, *851*, 83, [[arXiv:astro-ph.SR/1711.03974](#)]. <https://doi.org/10.3847/1538-4357/aa97e2>.
228. Evans, Neal J., I.; Dunham, M.M.; Jørgensen, J.K.; Enoch, M.L.; Merín, B.; van Dishoeck, E.F.; Alcalá, J.M.; Myers, P.C.; Stapelfeldt, K.R.; Huard, T.L.; et al. The Spitzer c2d Legacy Results: Star-Formation Rates and Efficiencies; Evolution and Lifetimes. *ApJS* **2009**, *181*, 321–350, [[arXiv:astro-ph/0811.1059](#)]. <https://doi.org/10.1088/0067-0049/181/2/321>.
229. Tobin, J.J.; Kratter, K.M.; Persson, M.V.; Looney, L.W.; Dunham, M.M.; Segura-Cox, D.; Li, Z.Y.; Chandler, C.J.; Sadavoy, S.I.; Harris, R.J.; et al. A triple protostellar system formed via fragmentation of a gravitationally unstable disk. *Nature* **2016**, *538*, 483–486, [[arXiv:astro-ph.SR/1610.08524](#)]. <https://doi.org/10.1038/nature20094>.
230. Wang, H.; Apai, D.; Henning, T.; Pascucci, I. FU Orionis: A Binary Star? *ApJ* **2004**, *601*, L83–L86, [[arXiv:astro-ph/astro-ph/0311606](#)]. <https://doi.org/10.1086/381705>.
231. Hales, A.S.; Corder, S.A.; Dent, W.R.D.; Andrews, S.M.; Eisner, J.A.; Cieza, L.A. The Early ALMA View of the FU Ori Outburst System. *ApJ* **2015**, *812*, 134, [[arXiv:astro-ph.SR/1509.02543](#)]. <https://doi.org/10.1088/0004-637X/812/2/134>.
232. Menard, F.; Monin, J.L.; Angelucci, F.; Rouan, D. Disks around Pre-Main-Sequence Binary Systems: The Case of Haro 6-10. *ApJ* **1993**, *414*, L117. <https://doi.org/10.1086/187010>.
233. Doppmann, G.W.; Najita, J.R.; Carr, J.S. Stellar and Circumstellar Properties of the Pre-Main-Sequence Binary GV Tau from Infrared Spectroscopy. *ApJ* **2008**, *685*, 298–312, [[arXiv:astro-ph/0805.2426](#)]. <https://doi.org/10.1086/590328>.
234. Nogueira, P.H.; Zurlo, A.; Pérez, S.; González-Ruiz, C.; Cieza, L.A.; Hales, A.; Bhowmik, T.; Ruiz-Rodríguez, D.A.; Principe, D.A.; Herczeg, G.J.; et al. Resolving the binary components of the outbursting protostar HBC 494 with ALMA. *MNRAS* **2023**, *523*, 4970–4991, [[arXiv:astro-ph.SR/2305.15647](#)]. <https://doi.org/10.1093/mnras/stad1614>.
235. Böhm, T.; Catala, C.; Balona, L.; Carter, B. Spectroscopic monitoring of the Herbig Ae star HD 104237. I. Multiperiodic stellar oscillations. *A&A* **2004**, *427*, 907–922. <https://doi.org/10.1051/0004-6361:20041227>.
236. Tatulli, E.; Isella, A.; Natta, A.; Testi, L.; Marconi, A.; Malbet, F.; Stee, P.; Petrov, R.G.; Millour, F.; Chelli, A.; et al. Constraining the wind launching region in Herbig Ae stars: AMBER/VLTI spectroscopy of HD 104237. *A&A* **2007**, *464*, 55–58, [[arXiv:astro-ph/astro-ph/0606684](#)]. <https://doi.org/10.1051/0004-6361:20065719>.
237. Kalas, P.G.; Rajan, A.; Wang, J.J.; Millar-Blanchaer, M.A.; Duchene, G.; Chen, C.; Fitzgerald, M.P.; Dong, R.; Graham, J.R.; Patience, J.; et al. Direct Imaging of an Asymmetric Debris Disk in the HD 106906 Planetary System. *ApJ* **2015**, *814*, 32, [[arXiv:astro-ph.EP/1510.02747](#)]. <https://doi.org/10.1088/0004-637X/814/1/32>.
238. Lagrange, A.M.; Langlois, M.; Gratton, R.; Maire, A.L.; Milli, J.; Olofsson, J.; Vigan, A.; Bailey, V.; Mesa, D.; Chauvin, G.; et al. A narrow, edge-on disk resolved around HD 106906 with SPHERE. *A&A* **2016**, *586*, L8, [[arXiv:astro-ph.SR/1510.02511](#)]. <https://doi.org/10.1051/0004-6361/201527264>.
239. Kennedy, G.M. Nature or nurture of coplanar Tatooines: the aligned circumbinary Kuiper Belt analogue around HD 131511. *MNRAS* **2015**, *447*, L75–L79, [[arXiv:astro-ph.EP/1412.0674](#)]. <https://doi.org/10.1093/mnrasl/slu190>.
240. Rich, E.A.; Monnier, J.D.; Aarnio, A.; Laws, A.S.E.; Setterholm, B.R.; Wilner, D.J.; Calvet, N.; Harries, T.; Miller, C.; Davies, C.L.; et al. Gemini-LIGHTS: Herbig Ae/Be and Massive T Tauri Protoplanetary Disks Imaged with Gemini Planet Imager. *AJ* **2022**, *164*, 109, [[arXiv:astro-ph.EP/2206.05815](#)]. <https://doi.org/10.3847/1538-3881/ac7be4>.
241. Müller, A.; Carmona, A.; van den Ancker, M.E.; van Boekel, R.; Henning, T.; Launhardt, R. HD 144432: A young triple system. *A&A* **2011**, *535*, L3, [[arXiv:astro-ph.SR/1110.2676](#)]. <https://doi.org/10.1051/0004-6361/201117971>.
242. Varga, J.; Waters, L.B.F.M.; Hogerheijde, M.; van Boekel, R.; Matter, A.; Lopez, B.; Perraut, K.; Chen, L.; Nadella, D.; Wolf, S.; et al. Mid-infrared evidence for iron-rich dust in the multi-ringed inner disk of HD 144432. *A&A* **2024**, *681*, A47, [[arXiv:astro-ph.SR/2401.03437](#)]. <https://doi.org/10.1051/0004-6361/202347535>.
243. Garufi, A.; Avenhaus, H.; Pérez, S.; Quanz, S.P.; van Holstein, R.G.; Bertrang, G.H.M.; Casassus, S.; Cieza, L.; Principe, D.A.; van der Plas, G.; et al. Disks Around T Tauri Stars with SPHERE (DARTTS-S). II. Twenty-one new polarimetric images of young stellar disks. *A&A* **2020**, *633*, A82, [[arXiv:astro-ph.EP/1911.10853](#)]. <https://doi.org/10.1051/0004-6361/201936946>.
244. Li, W.; Evans, Neal J., I.; Harvey, P.M.; Colome, C. Near-Infrared (J, H, K) Imaging of Herbig Ae/Be Stars. *ApJ* **1994**, *433*, 199. <https://doi.org/10.1086/174636>.
245. Millan-Gabet, R.; Schloerb, F.P.; Traub, W.A. Spatially Resolved Circumstellar Structure of Herbig AE/BE Stars in the Near-Infrared. *ApJ* **2001**, *546*, 358–381, [[arXiv:astro-ph/astro-ph/0008072](#)]. <https://doi.org/10.1086/318239>.

246. Monnier, J.D.; Berger, J.P.; Millan-Gabet, R.; Traub, W.A.; Schloerb, F.P.; Pedretti, E.; Benisty, M.; Carleton, N.P.; Haguenauer, P.; Kern, P.; et al. Few Skewed Disks Found in First Closure-Phase Survey of Herbig Ae/Be Stars. *ApJ* **2006**, *647*, 444–463, [[arXiv:astro-ph/astro-ph/0606052](#)]. <https://doi.org/10.1086/505340>.
247. Torres, G. A Double-lined Spectroscopic Orbit for the Young Star HD 34700. *AJ* **2004**, *127*, 1187–1193, [[arXiv:astro-ph/astro-ph/0311183](#)]. <https://doi.org/10.1086/381066>.
248. Monnier, J.D.; Harries, T.J.; Bae, J.; Setterholm, B.R.; Laws, A.; Aarnio, A.; Adams, F.C.; Andrews, S.; Calvet, N.; Espaillat, C.; et al. Multiple Spiral Arms in the Disk around Intermediate-mass Binary HD 34700A. *ApJ* **2019**, *872*, 122, [[arXiv:astro-ph.EP/1901.02467](#)]. <https://doi.org/10.3847/1538-4357/aafe87>.
249. Stapper, L.M.; Hogerheijde, M.R.; van Dishoeck, E.F.; Lin, L.; Ahmadi, A.; Booth, A.S.; Grant, S.L.; Immer, K.; Leemker, M.; Pérez-Sánchez, A.F. Constraining the gas mass of Herbig disks using CO isotopologues. *A&A* **2024**, *682*, A149, [[arXiv:astro-ph.EP/2312.03835](#)]. <https://doi.org/10.1051/0004-6361/202347271>.
250. Comerón, F.; Reipurth, B.; Yen, H.W.; Connelley, M.S. Binary energy source of the HH 250 outflow and its circumstellar environment. *A&A* **2018**, *612*, A73, [[arXiv:astro-ph.SR/1801.06939](#)]. <https://doi.org/10.1051/0004-6361/201730917>.
251. Stapelfeldt, K.R.; Duchêne, G.; Perrin, M.; Wolff, S.; Krist, J.E.; Padgett, D.L.; Ménard, F.; Pinte, C. HST Imaging of New Edge-on Circumstellar Disks in Nearby Star-forming Regions. In Proceedings of the Exploring the Formation and Evolution of Planetary Systems; Booth, M.; Matthews, B.C.; Graham, J.R., Eds., January 2014, Vol. 299, *IAU Symposium*, pp. 99–103. <https://doi.org/10.1017/S1743921313008004>.
252. Stapelfeldt, K.R.; Krist, J.E.; Ménard, F.; Bouvier, J.; Padgett, D.L.; Burrows, C.J. An Edge-On Circumstellar Disk in the Young Binary System HK Tauri. *ApJ* **1998**, *502*, L65–L69. <https://doi.org/10.1086/311479>.
253. Wölfer, L.; Facchini, S.; van der Marel, N.; van Dishoeck, E.F.; Benisty, M.; Bohn, A.J.; Francis, L.; Izquierdo, A.F.; Teague, R.D. Kinematics and brightness temperatures of transition discs. A survey of gas substructures as seen with ALMA. *A&A* **2023**, *670*, A154, [[arXiv:astro-ph.EP/2208.09494](#)]. <https://doi.org/10.1051/0004-6361/202243601>.
254. Simon, M.; Chen, W.P.; Howell, R.R.; Benson, J.A.; Slowik, D. Multiplicity among the Young Stars in Taurus. *ApJ* **1992**, *384*, 212. <https://doi.org/10.1086/170864>.
255. Stapelfeldt, K.R.; Ménard, F.; Watson, A.M.; Krist, J.E.; Dougados, C.; Padgett, D.L.; Brandner, W. Hubble Space Telescope WFPC2 Imaging of the Disk and Jet of HV Tauri C. *ApJ* **2003**, *589*, 410–418. <https://doi.org/10.1086/374374>.
256. Ruíz-Rodríguez, D.; Ireland, M.; Cieza, L.; Kraus, A. The frequency of binary star interlopers amongst transitional discs. *MNRAS* **2016**, *463*, 3829–3847, [[arXiv:astro-ph.SR/1609.02979](#)]. <https://doi.org/10.1093/mnras/stw2297>.
257. Ruíz-Rodríguez, D.; Cieza, L.A.; Williams, J.P.; Andrews, S.M.; Principe, D.A.; Caceres, C.; Canovas, H.; Casassus, S.; Schreiber, M.R.; Kastner, J.H. ALMA survey of circumstellar discs in the young stellar cluster IC 348. *MNRAS* **2018**, *478*, 3674–3692, [[arXiv:astro-ph.SR/1805.07590](#)]. <https://doi.org/10.1093/mnras/sty1351>.
258. Enoch, M.L.; Evans, Neal J., I.; Sargent, A.I.; Glenn, J. Properties of the Youngest Protostars in Perseus, Serpens, and Ophiuchus. *ApJ* **2009**, *692*, 973–997, [[arXiv:astro-ph/0809.4012](#)]. <https://doi.org/10.1088/0004-637X/692/2/973>.
259. Barber, M.G.; Mann, A.W.; Vanderburg, A.; Krolkowski, D.; Kraus, A.; Ansdel, M.; Pearce, L.; Mace, G.N.; Andrews, S.M.; Boyle, A.W.; et al. A giant planet transiting a 3-Myr protostellar with a misaligned disk. *Nature* **2024**, *635*, 574–577, [[arXiv:astro-ph.EP/2411.18683](#)]. <https://doi.org/10.1038/s41586-024-08123-3>.
260. Glauser, A.M.; Ménard, F.; Pinte, C.; Duchêne, G.; Güdel, M.; Monin, J.L.; Padgett, D.L. Multiwavelength studies of the gas and dust disc of IRAS 04158+2805. *A&A* **2008**, *485*, 531–540, [[arXiv:astro-ph/0804.3483](#)]. <https://doi.org/10.1051/0004-6361:20065685>.
261. Wootten, A. The Duplicity of IRAS 16293-2422: A Protobinary Star? *ApJ* **1989**, *337*, 858. <https://doi.org/10.1086/167156>.
262. Maureira, M.J.; Pineda, J.E.; Segura-Cox, D.M.; Caselli, P.; Testi, L.; Lodato, G.; Loinard, L.; Hernández-Gómez, A. Orbital and Mass Constraints of the Young Binary System IRAS 16293-2422 A. *ApJ* **2020**, *897*, 59, [[arXiv:astro-ph.SR/2005.11954](#)]. <https://doi.org/10.3847/1538-4357/ab960b>.
263. Kraus, S.; Kluska, J.; Kreplin, A.; Bate, M.; Harries, T.; Hofmann, K.H.; Hone, E.; Monnier, J.; Weigelt, G.; Anugu, N.; et al. VLTI Imaging of a High-Mass Protobinary System: Unveiling the Dynamical Processes in High-Mass Star Formation. *The Messenger* **2017**, *170*, 45–49. <https://doi.org/10.18727/0722-6691/5054>.
264. Girart, J.M.; Rodríguez, L.F.; Curiel, S. A Subarcsecond Binary Radio Source Associated with the X-Ray-Emitting Young Stellar Object YLW 15. *ApJ* **2000**, *544*, L153–L156. <https://doi.org/10.1086/317302>.
265. Brinch, C.; Jørgensen, J.K.; Hogerheijde, M.R.; Nelson, R.P.; Gressel, O. Misaligned Disks in the Binary Protostar IRS 43. *ApJ* **2016**, *830*, L16, [[arXiv:astro-ph.SR/1610.03626](#)]. <https://doi.org/10.3847/2041-8205/830/1/L16>.
266. Cieza, L.A.; González-Ruiz, C.; Hales, A.S.; Pinilla, P.; Ruiz-Rodríguez, D.; Zurlo, A.; Casassus, S.; Pérez, S.; Cánovas, H.; Arce-Tord, C.; et al. The Ophiuchus DISC Survey Employing ALMA (ODISEA) - III. The evolution of substructures in massive discs at 3–5 au resolution. *MNRAS* **2021**, *501*, 2934–2953, [[arXiv:astro-ph.EP/2012.00189](#)]. <https://doi.org/10.1093/mnras/staa3787>.
267. Long, F.; Herczeg, G.J.; Pascucci, I.; Apai, D.; Henning, T.; Manara, C.F.; Mulders, G.D.; Szűcs, L.; Helder, N.P. An ALMA Survey of Faint Disks in the Chamaeleon I Star-forming Region: Why Are Some Class II Disks so Faint? *ApJ* **2018**, *863*, 61, [[arXiv:astro-ph.SR/1806.04826](#)]. <https://doi.org/10.3847/1538-4357/aacce9>.
268. Carpenter, J.M.; Ricci, L.; Isella, A. An ALMA Continuum Survey of Circumstellar Disks in the Upper Scorpius OB Association. *ApJ* **2014**, *787*, 42, [[arXiv:astro-ph.SR/1404.0387](#)]. <https://doi.org/10.1088/0004-637X/787/1/42>.

269. Ansdell, M.; Williams, J.P.; van der Marel, N.; Carpenter, J.M.; Guidi, G.; Hogerheijde, M.; Mathews, G.S.; Manara, C.F.; Miotello, A.; Natta, A.; et al. ALMA Survey of Lupus Protoplanetary Disks. I. Dust and Gas Masses. *ApJ* **2016**, *828*, 46, [arXiv:astro-ph.EP/1604.05719]. <https://doi.org/10.3847/0004-637X/828/1/46>.
270. Ansdell, M.; Williams, J.P.; Trapman, L.; van Terwisga, S.E.; Facchini, S.; Manara, C.F.; van der Marel, N.; Miotello, A.; Tazzari, M.; Hogerheijde, M.; et al. ALMA Survey of Lupus Protoplanetary Disks. II. Gas Disk Radii. *ApJ* **2018**, *859*, 21, [arXiv:astro-ph.EP/1803.05923]. <https://doi.org/10.3847/1538-4357/aab890>.
271. Hamilton, C.M.; Herbst, W.; Shih, C.; Ferro, A.J. Eclipses by a Circumstellar Dust Feature in the Pre-main-Sequence Star KH 15D. *ApJ* **2001**, *554*, L201–L204, [arXiv:astro-ph/astro-ph/0105412]. <https://doi.org/10.1086/321707>.
272. Johnson, J.A.; Marcy, G.W.; Hamilton, C.M.; Herbst, W.; Johns-Krull, C.M. KH 15D: A Spectroscopic Binary. *AJ* **2004**, *128*, 1265–1272, [arXiv:astro-ph/astro-ph/0403099]. <https://doi.org/10.1086/422735>.
273. Chiang, E.I.; Murray-Clay, R.A. The Circumbinary Ring of KH 15D. *ApJ* **2004**, *607*, 913–920, [arXiv:astro-ph/astro-ph/0312515]. <https://doi.org/10.1086/383522>.
274. Leinert, C.; Richichi, A.; Haas, M. Binaries among Herbig Ae/Be stars. *A&A* **1997**, *318*, 472–484.
275. Reipurth, B. Disintegrating Multiple Systems in Early Stellar Evolution. *AJ* **2000**, *120*, 3177–3191. <https://doi.org/10.1086/316865>.
276. Reipurth, B.; Rodríguez, L.F.; Anglada, G.; Bally, J. Radio Continuum Maps of Deeply Embedded Protostars: Thermal Jets, Multiplicity, and Variability. *AJ* **2002**, *124*, 1045–1053. <https://doi.org/10.1086/341172>.
277. Takakuwa, S.; Saito, M.; Lim, J.; Saigo, K.; Sridharan, T.K.; Patel, N.A. A Keplerian Circumbinary Disk around the Protostellar System L1551 NE. *ApJ* **2012**, *754*, 52, [arXiv:astro-ph.GA/1205.3854]. <https://doi.org/10.1088/0004-637X/754/1/52>.
278. Kraus, A.L.; Ireland, M.J.; Martinache, F.; Hillenbrand, L.A. Mapping the Shores of the Brown Dwarf Desert. II. Multiple Star Formation in Taurus-Auriga. *ApJ* **2011**, *731*, 8, [arXiv:astro-ph.SR/1101.4016]. <https://doi.org/10.1088/0004-637X/731/1/8>.
279. Harris, R.J.; Andrews, S.M.; Wilner, D.J.; Kraus, A.L. A Resolved Census of Millimeter Emission from Taurus Multiple Star Systems. *ApJ* **2012**, *751*, 115, [arXiv:astro-ph.SR/1203.6353]. <https://doi.org/10.1088/0004-637X/751/2/115>.
280. Rodríguez, L.F.; Anglada, G.; Curiel, S. The Nature of the Radio Continuum Sources Embedded in the HH 7-11 Region and Its Surroundings. *ApJS* **1999**, *125*, 427–438. <https://doi.org/10.1086/313283>.
281. Mathieu, R.D.; Walter, F.M.; Myers, P.C. The Discovery of Six Pre-Main-Sequence Spectroscopic Binaries. *AJ* **1989**, *98*, 987. <https://doi.org/10.1086/115191>.
282. Lee, C.W.; Martin, E.L.; Mathieu, R.D. Relative Lithium Abundances in Pre-Main-Sequence Spectroscopic Binaries. *AJ* **1994**, *108*, 1445. <https://doi.org/10.1086/117168>.
283. Barsony, M.; Koresko, C.; Matthews, K. A Search for Close Binaries in the  $\rho$  Ophiuchi Star-forming Region. *ApJ* **2003**, *591*, 1064–1074, [arXiv:astro-ph/0303595]. <https://doi.org/10.1086/375532>.
284. Cabrit, S.; Pety, J.; Pesenti, N.; Dougados, C. Tidal stripping and disk kinematics in the RW Aurigae system. *A&A* **2006**, *452*, 897–906. <https://doi.org/10.1051/0004-6361:20054047>.
285. Rodriguez, J.E.; Loomis, R.; Cabrit, S.; Haworth, T.J.; Facchini, S.; Dougados, C.; Booth, R.A.; Jensen, E.L.N.; Clarke, C.J.; Stassun, K.G.; et al. Multiple Stellar Flybys Sculpting the Circumstellar Architecture in RW Aurigae. *ApJ* **2018**, *859*, 150, [arXiv:astro-ph.SR/1804.09190]. <https://doi.org/10.3847/1538-4357/aac08f>.
286. Kraus, S.; Hofmann, K.H.; Malbet, F.; Meilland, A.; Natta, A.; Schertl, D.; Stee, P.; Weigelt, G. Revealing the sub-AU asymmetries of the inner dust rim in the disk around the Herbig Ae star R Coronae Australinae. *A&A* **2009**, *508*, 787–803, [arXiv:astro-ph.SR/0911.3653]. <https://doi.org/10.1051/0004-6361/200912990>.
287. Mesa, D.; Bonnefoy, M.; Gratton, R.; Van Der Plas, G.; D’Orazi, V.; Sissa, E.; Zurlo, A.; Rigliaco, E.; Schmidt, T.; Langlois, M.; et al. Exploring the R CrA environment with SPHERE. Discovery of a new stellar companion. *A&A* **2019**, *624*, A4, [arXiv:astro-ph.SR/1902.02536]. <https://doi.org/10.1051/0004-6361/201834682>.
288. Correia, S.; Zinnecker, H.; Ratzka, T.; Sterzik, M.F. A VLT/NACO survey for triple and quadruple systems among visual pre-main sequence binaries. *A&A* **2006**, *459*, 909–926, [arXiv:astro-ph/0608674]. <https://doi.org/10.1051/0004-6361:20065545>.
289. Andrews, S.M.; Williams, J.P. Submillimeter Array Observations of Disks in the SR 24 Multiple Star System. *ApJ* **2005**, *619*, L175–L178, [arXiv:astro-ph/0411131]. <https://doi.org/10.1086/427325>.
290. Mayama, S.; Tamura, M.; Hanawa, T.; Matsumoto, T.; Ishii, M.; Pyo, T.S.; Suto, H.; Naoi, T.; Kudo, T.; Hashimoto, J.; et al. Direct Imaging of Bridged Twin Protoplanetary Disks in a Young Multiple Star. *Science* **2010**, *327*, 306. <https://doi.org/10.1126/science.1179679>.
291. Miley, J.M.; Carpenter, J.; Booth, R.; Jennings, J.; Haworth, T.J.; Vioque, M.; Andrews, S.; Wilner, D.; Benisty, M.; Huang, J.; et al. High-resolution ALMA observations of compact discs in the wide-binary system Sz 65 and Sz 66. *A&A* **2024**, *682*, A55, [arXiv:astro-ph.EP/2402.01903]. <https://doi.org/10.1051/0004-6361/202347135>.
292. Sanchis, E.; Testi, L.; Natta, A.; Manara, C.F.; Ercolano, B.; Preibisch, T.; Henning, T.; Facchini, S.; Miotello, A.; de Gregorio-Monsalvo, I.; et al. Demographics of disks around young very low-mass stars and brown dwarfs in Lupus. *A&A* **2020**, *633*, A114, [arXiv:astro-ph.SR/1911.06005]. <https://doi.org/10.1051/0004-6361/201936913>.
293. van’t Hoff, M.L.R.; Harsono, D.; Tobin, J.J.; Bosman, A.D.; van Dishoeck, E.F.; Jørgensen, J.K.; Miotello, A.; Murillo, N.M.; Walsh, C. Temperature Structures of Embedded Disks: Young Disks in Taurus Are Warm. *ApJ* **2020**, *901*, 166. <https://doi.org/10.3847/1538-4357/abb1a2>.
294. Muzerolle, J.; Calvet, N.; Briceño, C.; Hartmann, L.; Hillenbrand, L. Disk Accretion in the 10 MYR Old T Tauri Stars TW Hydreae and Hen 3-600A. *ApJ* **2000**, *535*, L47–L50. <https://doi.org/10.1086/312691>.

295. Torres, G.; Guenther, E.W.; Marschall, L.A.; Neuhäuser, R.; Latham, D.W.; Stefanik, R.P. Radial Velocity Survey of Members and Candidate Members of the TW Hydriæ Association. *AJ* **2003**, *125*, 825–841, [arXiv:astro-ph/astro-ph/0211157]. <https://doi.org/10.1086/345968>.
296. Duchêne, G.; Bouvier, J.; Simon, T. Low-mass binaries in the young cluster IC 348: implications for binary formation and evolution. *A&A* **1999**, *343*, 831–840, [arXiv:astro-ph/astro-ph/9901034]. <https://doi.org/10.48550/arXiv.astro-ph/9901034>.
297. Andrews, S.M.; Wilner, D.J.; Espaillat, C.; Hughes, A.M.; Dullemond, C.P.; McClure, M.K.; Qi, C.; Brown, J.M. Resolved Images of Large Cavities in Protoplanetary Transition Disks. *ApJ* **2011**, *732*, 42, [arXiv:astro-ph.GA/1103.0284]. <https://doi.org/10.1088/0004-637X/732/1/42>.
298. Eisner, J.A.; Lane, B.F.; Hillenbrand, L.A.; Akeson, R.L.; Sargent, A.I. Resolved Inner Disks around Herbig Ae/Be Stars. *ApJ* **2004**, *613*, 1049–1071, [arXiv:astro-ph/astro-ph/0406356]. <https://doi.org/10.1086/423314>.
299. Donati, J.F.; Cristofari, P.I.; Carmona, A.; Grankin, K. SPIRou monitoring of the protostar V347 Aur: binarity, magnetic fields, pulsed dynamo, and accretion. *MNRAS* **2024**, *534*, 231–250, [arXiv:astro-ph.SR/2407.05121]. <https://doi.org/10.1093/mnras/stae2076>.
300. Stempels, H.C.; Gahm, G.F. The close T Tauri binary V 4046 Sagittarii. *A&A* **2004**, *421*, 1159–1168. <https://doi.org/10.1051/0004-6361:20034502>.
301. Rosenfeld, K.A.; Andrews, S.M.; Wilner, D.J.; Stempels, H.C. A Disk-based Dynamical Mass Estimate for the Young Binary V4046 Sgr. *ApJ* **2012**, *759*, 119, [arXiv:astro-ph.SR/1209.4407]. <https://doi.org/10.1088/0004-637X/759/2/119>.
302. Duchêne, G.; Ghez, A.M.; McCabe, C.; Weinberger, A.J. No Fossil Disk in the T Tauri Multiple System V773 Tauri. *ApJ* **2003**, *592*, 288–298, [arXiv:astro-ph/astro-ph/0303648]. <https://doi.org/10.1086/375624>.
303. Torres, R.M.; Loinard, L.; Mioduszewski, A.J.; Boden, A.F.; Franco-Hernández, R.; Vlemmings, W.H.T.; Rodríguez, L.F. VLBA Determination of the Distance to nearby Star-forming Regions. V. Dynamical Mass, Distance, and Radio Structure of V773 Tau A. *ApJ* **2012**, *747*, 18, [arXiv:astro-ph.SR/1112.0114]. <https://doi.org/10.1088/0004-637X/747/1/18>.
304. Boden, A.F.; Torres, G.; Duchêne, G.; Konopacky, Q.; Ghez, A.M.; Torres, R.M.; Loinard, L. A Surprising Dynamical Mass for V773 Tau B. *ApJ* **2012**, *747*, 17, [arXiv:astro-ph.SR/1112.1018]. <https://doi.org/10.1088/0004-637X/747/1/17>.
305. Smith, K.W.; Balega, Y.Y.; Duschl, W.J.; Hofmann, K.H.; Lachaume, R.; Preibisch, T.; Schertl, D.; Weigelt, G. Close binary companions of the HAeBe stars LkH $\alpha$  198, Elias 1, HK Ori and V380 Ori. *A&A* **2005**, *431*, 307–319, [arXiv:astro-ph/astro-ph/0410449]. <https://doi.org/10.1051/0004-6361:20041135>.
306. Monnier, J.D.; Tannirkulam, A.; Tuthill, P.G.; Ireland, M.; Cohen, R.; Danchi, W.C.; Baron, F. Discovery of a Circumbinary Disk around Herbig Ae/Be System V892 Tauri. *ApJ* **2008**, *681*, L97, [arXiv:astro-ph/0807.0146]. <https://doi.org/10.1086/590532>.
307. Murillo, N.M.; Lai, S.P.; Bruderer, S.; Harsono, D.; van Dishoeck, E.F. A Keplerian disk around a Class 0 source: ALMA observations of VLA1623A. *A&A* **2013**, *560*, A103, [arXiv:astro-ph.GA/1310.8481]. <https://doi.org/10.1051/0004-6361/201322537>.
308. Harris, R.J.; Cox, E.G.; Looney, L.W.; Li, Z.Y.; Yang, H.; Fernández-López, M.; Kwon, W.; Sadavoy, S.; Segura-Cox, D.; Stephens, I.; et al. ALMA Observations of Polarized 872  $\mu$ m Dust Emission from the Protostellar Systems VLA 1623 and L1527. *ApJ* **2018**, *861*, 91, [arXiv:astro-ph.SR/1805.08792]. <https://doi.org/10.3847/1538-4357/aac6ec>.
309. Plavchan, P.; Gee, A.H.; Stapelfeldt, K.; Becker, A. The Peculiar Periodic YSO WL 4 in  $\rho$  Ophiuchus. *ApJ* **2008**, *684*, L37, [arXiv:astro-ph/0807.4557]. <https://doi.org/10.1086/592107>.
310. Ressler, M.E.; Barsony, M. A Cold Luminous Object in the Triple System WL20. In Proceedings of the IAU Symposium; Reipurth, B.; Zinnecker, H., Eds., January 2000, Vol. 200, *IAU Symposium*, p. 44.
311. Barsony, M.; Ressler, M.E.; Le Gouellec, V.J.M.; Tychoniec, Ł.; van Gelder, M.L. Resolving Twin Jets and Twin Disks with JWST and ALMA: The Young WL 20 Multiple System. *ApJ* **2024**, *973*, 42, [arXiv:astro-ph.SR/2409.03016]. <https://doi.org/10.3847/1538-4357/ad5da1>.
312. Kohn, S.A.; Shkolnik, E.L.; Weinberger, A.J.; Carlberg, J.K.; Llama, J. Searching for Spectroscopic Binaries within Transition Disk Objects. *ApJ* **2016**, *820*, 2, [arXiv:astro-ph.SR/1602.07582]. <https://doi.org/10.3847/0004-637X/820/1/2>.
313. Herczeg, G.J.; Brown, J.M.; van Dishoeck, E.F.; Pontoppidan, K.M. Disks and outflows in CO rovibrational emission from embedded, low-mass young stellar objects. *A&A* **2011**, *533*, A112, [arXiv:astro-ph.SR/1106.5391]. <https://doi.org/10.1051/0004-6361/201016246>.
314. Plavchan, P.; Güth, T.; Laohakunakorn, N.; Parks, J.R. The identification of 93 day periodic photometric variability for YSO YLW 16A. *A&A* **2013**, *554*, A110, [arXiv:astro-ph.SR/1304.2398]. <https://doi.org/10.1051/0004-6361/201220747>.
315. Dong, R.; Liu, H.B.; Cuello, N.; Pinte, C.; Ábrahám, P.; Vorobyov, E.; Hashimoto, J.; Kóspál, Á.; Chiang, E.; Takami, M.; et al. A likely flyby of binary protostar Z CMa caught in action. *Nature Astronomy* **2022**, *6*, 331–338, [arXiv:astro-ph.SR/2201.05617]. <https://doi.org/10.1038/s41550-021-01558-y>.

**Disclaimer/Publisher's Note:** The statements, opinions and data contained in all publications are solely those of the individual author(s) and contributor(s) and not of MDPI and/or the editor(s). MDPI and/or the editor(s) disclaim responsibility for any injury to people or property resulting from any ideas, methods, instructions or products referred to in the content.